Journal of Medicinal Chemistry

pubs.acs.org/jmc

Article

Synthesis and Pharmacological Evaluation of Novel Non-nucleotide Purine Derivatives as P2X7 Antagonists for the Treatment of Neuroinflammation

Francesco Calzaferri, Paloma Narros-Fernández, Ricardo de Pascual, Antonio M.G. de Diego, Annette Nicke, Javier Egea, Antonio G. García,* and Cristóbal de los Ríos*

Cite This: *J. Med. Chem.* 2021, 64, 2272−2290

Read Online

ACCESS | Metrics & More | Article Recommendations | Supporting Information

ABSTRACT: The ATP-gated P2X7 purinergic receptor (P2X7) is involved in the pathogenesis of many neurodegenerative diseases (NDDs). Several P2X7 antagonists have been developed, though none of them reached clinical trials for this indication. In this work, we designed and synthesized novel blood−brain barrier (BBB)-permeable derivatives as potential P2X7 antagonists. They comprise purine or xanthine cores linked to an aryl group through different short spacers. Compounds were tested in YO-PRO-1 uptake assays and intracellular calcium dynamics in a human P2X7-expressing HEK293 cell line, two-electrode voltage-clamp recordings in *Xenopus laevis* oocytes, and in interleukin 1β release assays in mouse peritoneal macrophages. BBB permeability was assessed by parallel artificial membrane permeability assays and P-glycoprotein ATPase activity. Dichloroarylpurinylethanones featured a certain P2X7 blockade, being compound **6** (2-(6-chloro-9*H*-purin-9-yl)-1-(2,4-dichlorophenyl)ethan-1-one), named ITH15004, the most potent, selective, and BBB-permeable antagonist. Compound **6** can be considered as a first non-nucleotide purine hit for future drug optimizations.

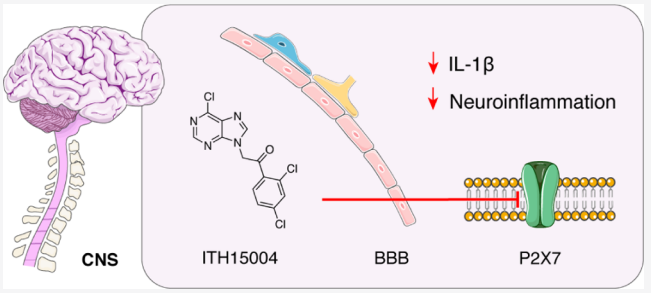

INTRODUCTION

Brain disorders affect 1 billion people around the world.[1] Neurodegenerative diseases (NDDs) are the most common form of brain disorder and, since they are age-dependent, this results in a high socio-economic burden as the longevity of the global population increases.[2] Current available medicines only mitigate some of the symptoms. For this reason, new innovative, more potent, and selective drugs are urgently needed to hinder disease progression. The NDDs, such as Alzheimer's disease (AD), Parkinson's disease (PD), amyotrophic lateral sclerosis (ALS), and multiple sclerosis (MS), feature diverse symptomatology and physiopathology. However, recent evidences focus on neuroinflammation as a common central stage in their pathogenesis.

In this context, the ATP-gated P2X7 purinergic ion channels (P2X7) are emerging as important gatekeepers of neuroinflammation[3] and as novel therapeutic targets for the above-mentioned diseases.[4] P2X7 is a non-selective ligand-operated ion channel, physiologically activated by ATP. They are permeable to Na^+, Ca^{2+}, and K^+ as well as to small molecules up to 900 Da of molecular weight.[5,6] P2X7s have a low affinity for ATP. Thus, they are considered as important sensors of tissue damage and inflammation, conditions where extracellular ATP levels considerably rise. P2X7 activation triggers immune responses that mediate maturation and secretion of interleukins, such as interleukin-1β (IL-1β).[7,8] Each P2X7 subunit is structurally characterized by a dolphin-like shape and assembles into homotrimers that present three extracellular ATP-binding pockets at the subunit interfaces.[9] Two main allosteric binding sites have been described so far,[10−12] which are located in the extracellular domain along the longitudinal axis of the receptor. Most of the antagonists developed so far bind to the allosteric pocket placed in the upper vestibule of the receptor, hindering the conformational changes that lead to the pore opening.

Concerning AD, an *in vivo* study using the Tg2576 AD mouse model reported that P2X7s are overexpressed in both astrocytes and microglia around Aβ senile plaques[13] as was also observed in AD patients.[14] Pharmacological inhibition of P2X7 using Brilliant Blue G (BBG) (Chart 1) in the transgenic J20 mice carrying the human APP protein induced a significant decrease of hippocampal amyloid plaques.[15] Moreover, the P2X7 antagonist GSK1482160 (Chart 1) reduced ATP-

Received: December 11, 2020
Published: February 9, 2021

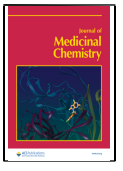

https://dx.doi.org/10.1021/acs.jmedchem.0c02145
J. Med. Chem. 2021, 64, 2272−2290

Chart 1. Chemical Structure of Some P2X7 Antagonists, Including the Adamantane-*o*-chlorobenzamide Scaffold Reported by Astra-Zeneca (1)[25]

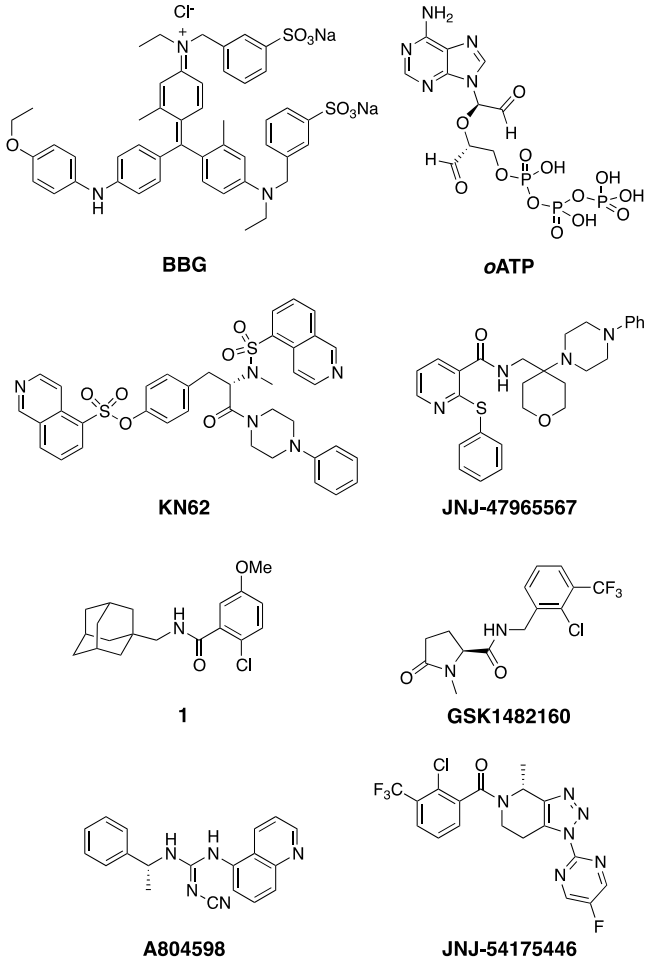

induced microglia migration and restored their phagocytic activity in mice.[14]

As for PD, P2X7s are overexpressed in PD patients,[16] and their activation is cytotoxic for dopaminergic SN4741 neurons.[17] BBG succeeded in preventing dopaminergic neuron loss in the 6-hydroxydopamine-injected rat model of PD.[18,19]

P2X7s have an important role in ALS neuroinflammation,[20] and their expression is up-regulated in the post-mortem spinal cord tissue of ALS patients.[21] The treatment with BBG improved motoneuron survival and motor performance deficit of the treated SOD1^{G93A} mice,[22] a disease model for ALS, though no effect was observed when JNJ-47965567 (Chart 1), a more potent and selective antagonist, was used.[23] Finally, a high expression of P2X7 in activated microglia and astrocytes of post-mortem MS patients has been reported.[21,24]

The earliest attempts to synthesize P2X7 antagonists based on nucleotide analogues resulted in the irreversible inhibitor *o*-ATP (Chart 1).[26] Then, the discovery of the triphenylmethane dye BBG, which is blood–brain barrier (BBB)-permeable[27] but a non-selective P2X7 antagonist, constituted a real breakthrough. Other first-generation P2X7 antagonists were the non-selective pyridoxalphosphate derivative PPADS,[28] the naphthylsulfonate suramine, and its isoquinoline derivative KN-62[29] (Chart 1). During the last 2 decades, the search for more potent, selective, and CNS-penetrant P2X7 antagonists has been a continuous challenge, which has led to a series of KN-62 derivatives,[30] the discovery of berberine alkaloids as P2X7 blockers,[31] and the development of adamantine-[32] and *o*-chlorobenzamide-based new ligands as well as their juxtaposition products (**1**, Chart 1).[25] Several other scaffolds have been explored, such as 4,5-diarylimidazolines,[33] pyrazolodiazepines,[34] 1-piperidinylimidazoles,[35] quinolones and quinolinones,[36,37] arylboronic acids,[38] thiadiazoles,[39] and tetrazoles, yielding the derivative A438079.[40] They all have different structural motifs, but we noticed that the *o*-chlorobenzamide and its isosteres are recurrent patterns. For instance, it is present in a series of triazole rings disclosed by Janssen[41] as well as in the pyroglutamic acid amide analogue GSK1482160 (Chart 1)[42] as a superior homologue and an inverse isostere. Also, the heteroaryl-cyanoguanidines A740003[43] and A804598 (Chart 1)[44] can be considered as *o*-chlorobenzamide isosteres since both the cyano group and ortho-halogen induce the dihedral torsion of the aromatic ring over the vicinal guanidine or carbonyl group, respectively. Finally, the two Janssen derivatives JNJ-55308942[45] and JNJ-54175446[46] (Chart 1) also contain an *o*-halobenzamide moiety. The former passed three phase I clinical trials,[47] while the latter is currently in a phase II trial for major depression.[48] Apart from this, the other few P2X7 antagonists that have entered clinical trials were intended for the treatment of peripheral disorders.[49,50] Hence, there is still a great need for defining accurate drug-like properties to target the CNS, such as sufficient lipophilicity and brain tissue half-life. Our research group has recently embarked on a project aiming at the development of new P2X7 antagonists with enhanced BBB penetration for the potential treatment of brain diseases such as NDDs. We designed a novel series of compounds that combined the essential structural features for their inhibitory capacity on P2X7: the presence of a heteroaromatic cycle bound to a halobenzene through a non-complex spacer (Figure 1).

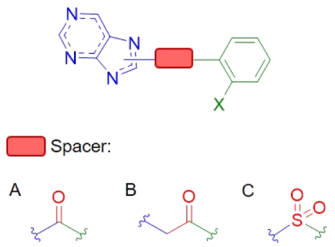

Figure 1. Scheme of the designed molecules. A purine scaffold (blue) was linked to an *o*-halophenyl (green) through three different spacers (red): carbonyl (A), ethanoyl (B), or sulfonyl (C) groups.

On this basis, we surprisingly noticed that the purine scaffold had been only explored in the earliest nucleotide P2X ligands,[51] but it had been never linked to the *o*-chlorobenzamide moiety. We then synthesized such non-nucleotide purine derivatives, hypothesizing that the halobenzamide substructure would afford potency and selectivity, whereas the purine-like heterocycles would contribute to favor BBB penetration.

RESULTS

Chemistry. Following the chemical design (Figure 1), several structures were proposed. At a first glance, the simplest design was based on connecting a purine analogue with *o*-chlorobenzamide through benzoylation. 6-Chloropurine was selected as a substrate to achieve regioselective nucleophilic

https://dx.doi.org/10.1021/acs.jmedchem.0c02145
J. Med. Chem. 2021, 64, 2272−2290

acyl substitution, assuming that chlorine at that position would hinder the N7 nucleophilic center. We first selected *o*-chlorobenzoic acid as the electrophile, assisted by cyanuric chloride,[52] unsuccessfully. With the use of *o*-chlorobenzoyl chloride as the acylating reagent, several bases, for example, pyridine or TEA, and solvents such as DMF, CH_2Cl_2, or MeCN were probed, achieving the best yield (78%) for the synthesis of **2** with the TEA/DMAP system as the base in THF (Scheme 1). Analogously, 6-methoxypurine (**3**), prepared by aromatic nucleophilic substitution with Na in MeOH, furnished benzoyl purine **4** in moderate yields (53%, Scheme 1).

Scheme 1. Synthesis of *o*-Chlorobenzoylpurines 2 and 4[a]

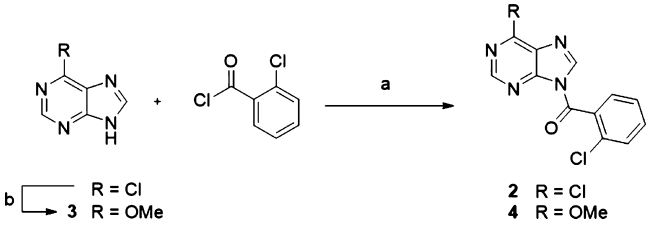

[a]Reagents and conditions: (a) TEA, DMAP, THF, 4.5−6 h, 0 °C to rt; (b) Na, MeOH, 2 h, 60 °C.

Subsequently, the homologous derivatives of *N*-acylpurines were synthesized to assess the effect of the spacer lengthening over the P2X7 antagonist capability and to improve the critical chemical stability (acid-catalyzed hydrolysis of the amide) of *N*-acylpurines. The nucleophilic substitution of 6-chloropurine on 2-chloro-1-(2,4-dichlorophenyl)ethan-1-one (**5**) assisted by NaH as the base in DMF afforded **6** (R^1, R^3, R^4 = Cl, R^2 = H, Scheme 2).

Scheme 2. Synthesis of Purinyl-2′,4′-disubstituted Phenylethanones (6 and 12−20)[a]

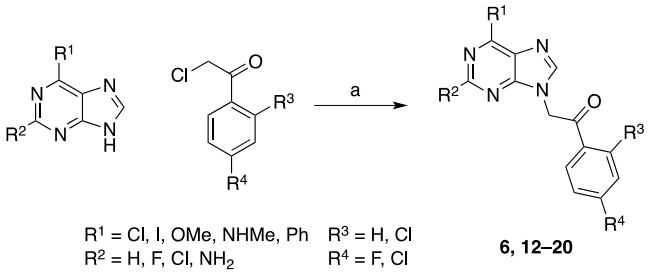

[a]Reagents and conditions. For the synthesis of **6** and **12−18**: (a) NaH, DMF, 15−40 h, 0 °C to rt. For the synthesis of **19**: (a) KOH, Bu_4NHSO_4, DMF, 26 h, 0 °C to rt. For the synthesis of **20**: (a) K_2CO_3, Bu_4NHSO_4, DMF, 30 h, 0 to 80 °C.

When tested on the selected pharmacological assays described below, purinylethanone **6** presented the most promising P2X7 antagonist profile. For this reason, we synthesized several new analogues of **6** to optimize its pharmacological properties (**12−20**). Modifications of **6** mainly pursued to probe the effect of substitution at C2 (R^2, Scheme 2) and the replacement of chlorine at C6 (R^1, Scheme 2). Compounds **12−20** were obtained in low to good yields (Table 2) following the experimental procedures depicted in Scheme 2. Compound **14** (R^1 = Ph, R^2 = H, R^3, R^4 = Cl, Scheme 2) was synthesized from 6-phenylpurine (**9**, Scheme S1, Supporting Information), easily accessible through Suzuki coupling of the THP-protected 6-chloropurine **7** with phenylboronic acid that gives rise to intermediate **8** and the subsequent deprotection to form 6-phenylpurine **9**. Compound **17** (R^1 = Cl, R^2 = F, R^3, R^4 = Cl, Scheme 2) was synthesized from 6-chloro-2-fluoropurine **10**, which was obtained from 6-chloropurin-2-amine and an HF solution in pyridine. Compound **18** (R^1 = I, R^2, R^3, R^4 = Cl, Scheme 2) was synthesized from 2-chloro-6-iodopurine **11**, which was prepared by treating 2,6-dichloropurine with HI. Compounds **19** and **20**, bearing a methylamine at C6 or an amine at C2, respectively, were prepared through nucleophilic substitution of commercial purines (2-chloro-*N*-methylpurin-6-amine and 6-chloropurin-2-amine, respectively) over the alkyl chloride **5**, assisted by tetrabutylammonium hydrogensulfate (TBAHS) phase transfer catalysis (Scheme 2). As expected, the presence of amines, susceptible to compete with N9 as nucleophile centers, lowered the chemical yield of the reactions (Table 2). X-ray analysis of **19** confirmed the expected regioselectivity of the reaction toward the N9-alkylation (Figure 2). To

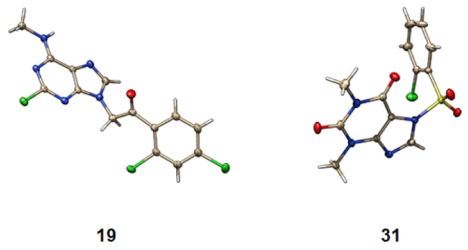

Figure 2. X-ray diffraction of compounds **19** and **31**. Purine and theophylline scaffolds used in this study have the same influence on N7 and N9 nucleophilicity for all the respective derivatives.

understand whether the chlorine at the ortho position was relevant for blocking the P2X7 opening, we synthesized other derivatives of compound **6** bearing only the halogen at the para position (R^3 = H, i.e., **12** and **13**, Scheme 2).

We also explored if lengthening the spacer present in compound **6** affected the pharmacological activity by inserting a propanone instead of an ethanone as the spacer between the purine core and the aryl group (Scheme 3). We prepared

Scheme 3. Synthesis of 3-(6-Chloro-9*H*-purin-9-yl)-1-(2′,4′-dichlorophenyl)-propan-1-one 22[a]

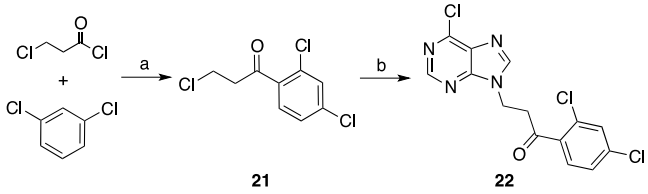

[a]Reagents and conditions: (a) $AlCl_3$, 4 h, rt to 60 °C; (b) 6-chloropurine, NaH, DMF, 18 h, 0 °C to rt.

compound **22** through a Friedel−Crafts reaction of 1,3-dichlorobenzene with 3-chloropropanoyl chloride to form intermediate **21** and the subsequent nucleophilic substitution with 6-chloropurine (Scheme 3).

Another strategy to modify the spacer and to improve the stability was the insertion of a sulfonamide moiety (Scheme 4), which is considered a non-classical bioisostere of amides. For this purpose, 6-chloropurine reacted with *o*-chlorobenzenesul-

https://dx.doi.org/10.1021/acs.jmedchem.0c02145
J. Med. Chem. 2021, 64, 2272−2290

Scheme 4. Synthesis of 2-Chlorophenylsulfonyl Purines (23−27)[a]

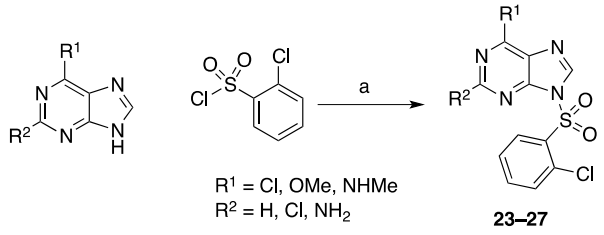

[a]Reagents and conditions: (a) TEA, DMAP, CH_2Cl_2/THF, 0 °C to rt, 2−4 h.

fonyl chloride to give **23** (R^1 = Cl, R^2 = H) in low yield when NaH was used as a base. Yield was enhanced (77%) by using the TEA/DMAP system (Scheme 4). Although compound **23** did not show a relevant P2X7 blockade (Table 1), we prepared

Table 1. P2X7 Antagonist Profile of the First Purine and Xanthine Derivatives Assessed by the YO-PRO-1 Aye Assay in hP2X7-HEK293 Cells and by TEVC in hP2X7-Expressing *X. laevis* Oocytes

compd.	scaffold	spacer	YO-PRO-1[a] (%)	I_{ATP}[c] (%)
JNJ			56 ± 5***	49 ± 4*
2	purine	−CO−	7 ± 2	5 ± 2
4	purine	−CO−	1 ± 8	0 ± 1
6	purine	$-CH_2CO-$	63 ± 4***[b]	47 ± 1***
23	purine	$-SO_2$	17 ± 6	9 ± 7
28	theobromine	−CO−	5 ± 10	5 ± 8
29	theobromine	$-CH_2CO-$	nb	2 ± 2
30	theophylline	$-CH_2CO-$	0 ± 8	10 ± 2
31	theophylline	$-SO_2-$	52 ± 4***[b]	28 ± 2**
40	purinone	$-CH_2-$	16 ± 6	9 ± 2

[a]hP2X7-HEK293 cells stimulated with BzATP 30 μM. Compound concentration was 10 μM, except for JNJ-47965567 (JNJ, 1 μM). Data are mean ± S.E.M. of triplicates of three different cultures. [b]IC_{50} data of **6** and **31** were calculated, being 9 ± 3 and 10 ± 4 μM, respectively. [c]Oocytes expressing hP2X7 stimulated with ATP 0.3 mM. Compound concentration was 100 μM, except for JNJ (1 μM). Data are mean ± S.E.M. of triplicates of three different oocytes from two different frogs. *P < 0.05, **p < 0.01, ***p < 0.001, nb = no blockade.

new purine derivatives bearing a sulfonyl spacer by considering the good biological results obtained with sulfonamide **31**. Thus, we replaced the chlorine at C6 of **23** (R^1, Scheme 4) by polar groups and evaluated the influence of substitutions at C2 (R^2, Scheme 4) over the pharmacological activity. Following the synthetic procedure provided in Scheme 4, analogues of compound **23** (**24**−**27**) were prepared in low to good yields and mild conditions.

The xanthine scaffold was also considered to build ligands under the chemical design outlined in Figure 1. Xanthine derivatives (e.g., theobromine, theophylline, caffeine, and so on) are substances with well-known CNS effects, thus eligible as the starting point to develop drugs with extended brain penetration. Hence, theobromine suffered benzoylation with *o*-chlorobenzoyl chloride under the conditions outlined in Scheme 5 to yield benzoyltheobromine **28** (Scheme 5).

Unlike 6-chloropurine, theobromine reacted better with **5** when using K_2CO_3 as the base in DMF at 150 °C under phase transfer catalysis (TBAHS) to form **29** (Scheme 5) presumably

Scheme 5. Synthesis of 2′,4′-Dichlorophenylethanones and 2′-Chlorobenzamides, Using Xanthine Derivatives as the Starting Material[a]

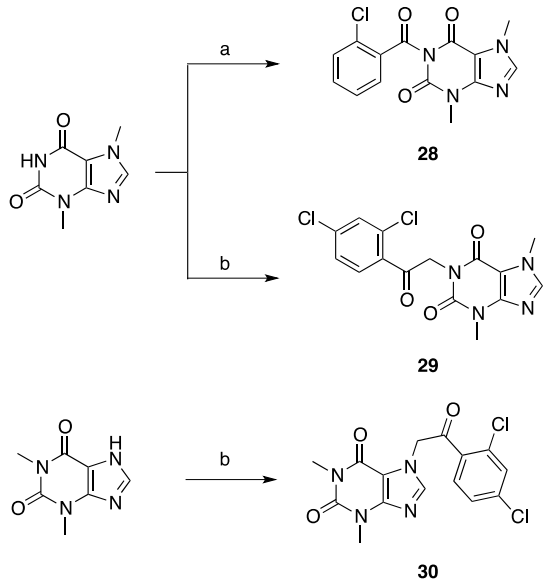

[a]Reagents and conditions: (a) 2-chlorobenzoyl chloride, TEA, DMAP, THF, 48 h, 0 to 70 °C; (b) 2-chloro-1-(2,4-dichlorophenyl)-ethan-1-one (**5**), K_2CO_3, Bu_4NHSO_4, DMF, 1−6 h, 150 °C.

due to the low nucleophilic strength of N1. Analogously but using theophylline as the starting material, we isolated **30** in moderate yields (Scheme 5, 45%). Only one of the two possible regioisomers was obtained. NOESY analysis did not show any spatial coupling between methylene and the methyl group at N3 (Figure S1, Supporting Information), confirming the more probable N7 alkylation.

The incorporation of the *o*-chlorophenylsulfonyl moiety to theophylline, following the procedure shown in Scheme 6, gave

Scheme 6. Synthesis of Arylsulfonyl Theophyllines (31−38)[a]

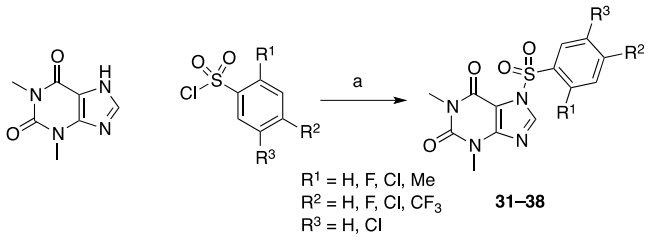

[a]Reagents and conditions: (a) NaH, THF, 4−48 h, 0 °C to rt.

31 in a regioselective fashion, as proved by X ray diffraction (Figure 2). We thus confirmed that N7 is the most nucleophilic center in theophylline as proposed for **30**. The theophylline **31** was the most promising analogue among the xanthine derivatives (Table 1). For this reason, we proposed tiny chemical modifications to increase its potency over P2X7. In this case, we focused on modifying substitutions at the pending phenyl ring (Scheme 6). Compounds **32**−**38** were obtained following the procedure shown in Scheme 6 with good yields.

Finally, to further explore possible modifications on the spacer and to evaluate whether a more stable amide than the

https://dx.doi.org/10.1021/acs.jmedchem.0c02145
J. Med. Chem. 2021, 64, 2272−2290

one present in benzoylpurines **2** and **4** could be essential for P2X7 antagonism, we designed a compound starting from 6-purinone and that included a methylene group as purinylarylethanones **6** and **12**−**20**. The result was the synthesis of **40** by nucleophilic substitution of 6-purinone **39**[53] over 1-chloro-2-(chloromethyl)benzene (Scheme 7).

Scheme 7. Synthesis of 2-Chloro-1-(2′-chlorobenzyl)-9-methyl-1,9-dihydro-6*H*-purin-6-one (40)[a]

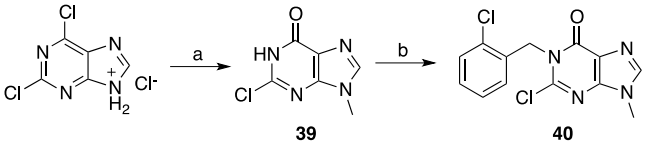

[a]Reagents and conditions: (a) basic alumina, MeOH, 24 h, 70 °C; (b) 1-chloro-2-(chloromethyl)benzene, $NaHCO_3$, DMF, overnight, 75 °C.

Biological Evaluation. Compounds **2**, **4**, **6**, **23**, **28**−**31**, and **40** were initially assessed as P2X7 antagonists by two experimental procedures, YO-PRO-1 dye uptake assay[54,55] and inhibition of ATP-activated currents in hP2X7-expressing *Xenopus laevis* oocytes (Table 1). In the former, the potent P2X7 agonist benzoyl-ATP (BzATP) activates the human P2X7 receptors (hP2X7), stably transfected in HEK293 cells. After channel opening, the dye enters the cell and binds to nucleic acids, giving a fluorescent signal. In the latter, ionic currents are evoked by ATP (300 μM) in the presence or absence of the assessed compounds to test their ability to inhibit channel opening. The percentages of blockade in both assays are shown in Table 1. JNJ-47965567 (Chart 1) was used as the reference P2X7 antagonist.

YO-PRO-1 uptake and ATP-activated currents were not affected by purines **2, 4, 23**, and the N1-benzyl-6-purinone **40**. By contrast, the ethanoyl spacer successfully contributed to the blockade of YO-PRO-1 uptake exerted by purine derivative **6** (63% at 10 μM, Table 1) but not in xanthine derivatives **29** and **30**. The sulfonyl spacer was only effective when linked to theophylline, as in **31**, which halves the YO-PRO-1 uptake at 10 μM and reduces ATP currents in hP2X7-expressing oocytes (Table 1). Those compounds possessing a %blockade of YO-PRO-1 uptake higher than 40% at 10 μM were subjected to concentration−response experiments. Thus, compounds **6** and **31** presented an IC_{50} defined as their concentration capable of reducing the BzATP-induced YO-PRO-1 uptake by 50% of 9 ± 3 and 10 ± 4 μM, respectively. Interestingly, the two screening methods confirmed each other's outcomes despite the experimental differences.

Considering the promising pharmacological profile of **6** as P2X7 antagonist, its analogues **12**−**20** were prepared and biologically assessed (Table 2). Most of the compounds **12**−**20** did not reach the blocking properties of their head compound **6** (Table 2), as measured by the YO-PRO-1 assay and two-electrode voltage-clamp (TEVC). Compounds **12**, **14**, and **16** presented an IC_{50} to block the BzATP-induced YO-PRO-1 uptake of 10 ± 2, 6 ± 1, and 13 ± 2 μM, respectively, comparable data to that of compound **6**. In any case, the use of the ethanoyl spacer seemed appropriate since most of them reduced the YO-PRO-1 uptake in a significant manner. Generally, we noticed that an increase in polarity of the substituents on the purine scaffold lowered the inhibitory potential. Moreover, hydrophobic bulky substituents at the C6 position (R^1) were well tolerated, like the phenyl present in **14**. By contrast, only the highly halogenated derivatives **16** and **17** showed a decent mitigation of the ATP-evoked currents,

Table 2. P2X7 Antagonist Profile of Purinylarylethanones 12−20, Analogues of 6, Assessed by the YO-PRO-1 Dye Uptake Assay in hP2X7-HEK293 Cells and by TEVC in hP2X7-Expressing *X. laevis* Oocytes

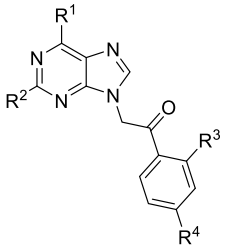

compd.	R^1	R^2	R^3	R^4	yield[a] (%)	YO-PRO-1[b] (%)	I_{ATP}[d] (%)
JNJ						56 ± 5***	49 ± 4**
6	Cl	H	Cl	Cl	45	63 ± 4***[c]	37 ± 1***
12	Cl	H	H	Cl	48	55 ± 4***[c]	11 ± 3
13	Cl	H	H	F	83	34 ± 7**	7 ± 2
14	Ph	H	Cl	Cl	41	62 ± 3***[c]	11 ± 2
15	MeO	H	Cl	Cl	28	25 ± 3***	14 ± 2*
16	Cl	Cl	Cl	Cl	40	41 ± 3***[c]	24 ± 2**
17	Cl	F	Cl	Cl	39	27 ± 5**	24 ± 3*
18	I	Cl	Cl	Cl	28	14 ± 4	6 ± 2
19	NHMe	Cl	Cl	Cl	22	2 ± 9	5 ± 7
20	Cl	NH_2	Cl	Cl	10	4 ± 16	6 ± 4

[a]Chemical yields of the reaction in Scheme 2. [b]hP2X7-HEK293 cells stimulated with BzATP 30 μM. Compounds assayed at 10 μM, except for JNJ-47965567 (JNJ, 1 μM). Data are mean ± S.E.M. of triplicates of three different cell cultures. [c]IC_{50} data of **6**, **12**, **14**, and **16** were calculated, being 9 ± 3, 10 ± 2, 6 ± 1, and 13 ± 2 μM, respectively. [d]Oocytes expressing the hP2X7 stimulated with ATP 0.3 mM. Compounds assayed at 100 μM, except for JNJ (1 μM). Data are mean ± S.E.M. of triplicates of three different oocytes from two different frogs. *$P < 0.05$, **$p < 0.01$, ***$p < 0.001$.

https://dx.doi.org/10.1021/acs.jmedchem.0c02145
J. Med. Chem. 2021, 64, 2272−2290

slightly worse than that exerted by compound **6**. Interestingly, substitutions at C2 (R^2) decreased ligands' potency, presumably due to steric effects since halogens are better tolerated than an amine, but no substitution still affords the best result.

According to ATP current data of compounds **12** and **13**, the removal of chlorine at C2′ of the aryl residue leads to a decrease in potency, meaning that the chlorine is necessary for antagonism, and confirming our hypothesis that an *o*-haloaryl moiety (or its structural isostere-like aryl-cyanoguanidine) is essential for the P2X7 blocking activity, as represented in the majority of P2X7 antagonists.

Compound **22**, the superior homologue of compound **6**, scarcely affected both YO-PRO-1 uptake (19 ± 9% blockade) and ATP currents (6 ± 1% blockade), indicating that lengthening the spacer is not beneficial to inhibit the P2X7. Hence, we did not launch further similar analogues.

As for analogues of arylsulfonylpurine **23** (**24**–**27**), the insertion of polar substituents hindered the P2X7 inhibition (Table 3). Apparently, the addition of a chlorine atom at C2

Table 3. P2X7 Antagonist Profile of 2-Chlorophenylsulfonylpurines 24–27, Analogues of 23, Assessed by the YO-PRO-1 Dye Uptake Assay in hP2X7-HEK293 Cells and by TEVC Analysis in hP2X7-Expressing *X. laevis* Oocytes

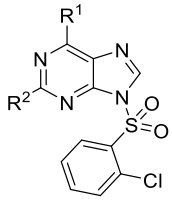

compd.	R^1	R^2	yield[a] (%)	YO-PRO-1[b] (%)	I_{ATP}[d] (%)
JNJ				56 ± 5***	49 ± 4*
23	Cl	H	77	17 ± 6	9 ± 7
24	Cl	Cl	47	46 ± 4**[c]	2 ± 1
25	MeO	H	37	nb	8 ± 8
26	Cl	NH_2	50	9 ± 9	Nb
27	NHMe	Cl	48	4 ± 8	2 ± 1

[a]Chemical yields of the reaction in Scheme 4. [b]hP2X7-HEK293 cells stimulated with BzATP 30 μM. Compounds assayed at 10 μM, except for JNJ-47965567 (JNJ, 1 μM). Data are mean ± S.E.M. of triplicates of three different cell cultures. [c]IC_{50} of **24** was calculated, being 10.2 ± 0.6 μM. [d]hP2X7-expressing oocytes stimulated with ATP 0.3 mM. Compounds assayed at 100 μM, except for JNJ (1 μM). Data are mean ± S.E.M. of triplicates of three different oocytes from two different frogs. *P < 0.05, **p < 0.01, ***p < 0.001, nb = no blockade.

(R^2 = Cl, Scheme 4), as in compound **24**, conferred potency to these derivatives according to the YO-PRO-1 assay. For this reason, its IC_{50} was calculated, being 10.2 ± 0.6 μM, a similar value to those found for the best compounds of these series. However, considering that these data were not confirmed by TEVC (Table 3), we speculate that the potency of compound **24** is not strictly related to P2X7 pore opening.

Derivatives **32**–**38** were prepared and pharmacologically assessed according to the apparent blocking properties of arylsulfonyltheophylline **31** (Scheme 6). However, they elicited a very weak blockade of P2X7 (Table 4). It seems that the substitution at the phenyl ring in the theophylline

Table 4. P2X7 Antagonist Profile of Arylsulfonyltheophyllines 32–38, Analogues of 31, Assessed by the YO-PRO-1 Dye Uptake Assay in hP2X7-HEK293 Cells and by TEVC Analysis in hP2X7-Expressing *X. laevis* Oocytes

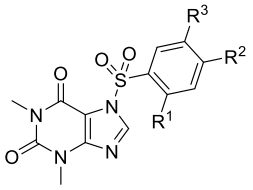

compd.	R_1	R_2	R_3	yield[a] (%)	YO-PRO-1[b] (%)	I_{ATP}[d] (%)
JNJ					56 ± 5***	49 ± 4*
31	Cl	H	H	69	52 ± 4***[c]	28 ± 2**
32	Cl	Cl	H	74	7 ± 3	9 ± 1
33	Cl	F	H	54	20 ± 4	nb
34	Cl	CF_3	H	75	5 ± 3	nb
35	F	F	H	72	7 ± 4	1 ± 2
36	Me	F	H	78	23 ± 7	nb
37	Cl	H	Cl	73	4 ± 5	nb
38	H	F	H	81	10 ± 1	nb

[a]Chemical yields of the reaction in Scheme 6. [b]hP2X7-HEK293 cells stimulated with BzATP 30 μM. Compounds assayed at 10 μM, except for JNJ-47965567 (JNJ, 1 μM). Data are mean ± S.E.M. of triplicates of three different cell cultures. [c]IC_{50} of **31** was calculated, being 10 ± 4 μM. [d]hP2X7-expressing oocytes stimulated with ATP 0.3 mM. Compounds assayed at 100 μM, except for JNJ (1 μM). Data are mean ± S.E.M. of triplicates of three different oocytes from two different frogs. *P < 0.05, **p < 0.01, ***p < 0.001.

subfamily dramatically impairs the favorable interactions of ligands with the binding site of the receptor.

Cytosolic Ca^{2+} concentration ($[Ca^{2+}]_c$) changes were assessed in the presence of most of the synthesized compounds to corroborate the pharmacological results acquired (Table S1, Supporting Information). The $[Ca^{2+}]_c$ was monitored in hP2X7-expressing HEK293 cells with the fluorescent dye FURA-2 after P2X7 activation by BzATP. Compound **6** showed the best receptor inhibition (Figure 3), in agreement with previous assays. It exerted a concentration-dependent P2X7 blockade with an IC_{50} of 13.7 μM. The activity of compound **14** in the Ca^{2+} dynamics assay is in line with the YO-PRO-1 data (Table S1, Supporting Information) but not with those of TEVC (Table 2). This incongruence could be ascribed to the high concentration used in the TEVC experiments, which would be reaching the solubility threshold of **14**.

The potency of a selection of the novel antagonists reported in this paper was then evaluated in a well-known model of P2X7-induced inflammation,[56,57] which is the quantification of IL-1β released by murine peritoneal macrophages (MPMs), after LPS priming, and ATP stimulation (Figure 4). Only compounds **6** and **31** reduced IL-1β release in a concentration-dependent fashion (Figure 4A,B, respectively), in agreement with their P2X7-blocking properties found in the previous assays. In addition, these experiments demonstrated that the two most promising hit compounds are also active on *Mus musculus* P2X7.

All the pharmacological data classified by chemical families have been collected and reorganized in Table S1 (Supporting Information). Since compound **6** stood out as the most potent P2X7 antagonist, we evaluated its selectivity in three rat P2X

https://dx.doi.org/10.1021/acs.jmedchem.0c02145
J. Med. Chem. 2021, 64, 2272–2290

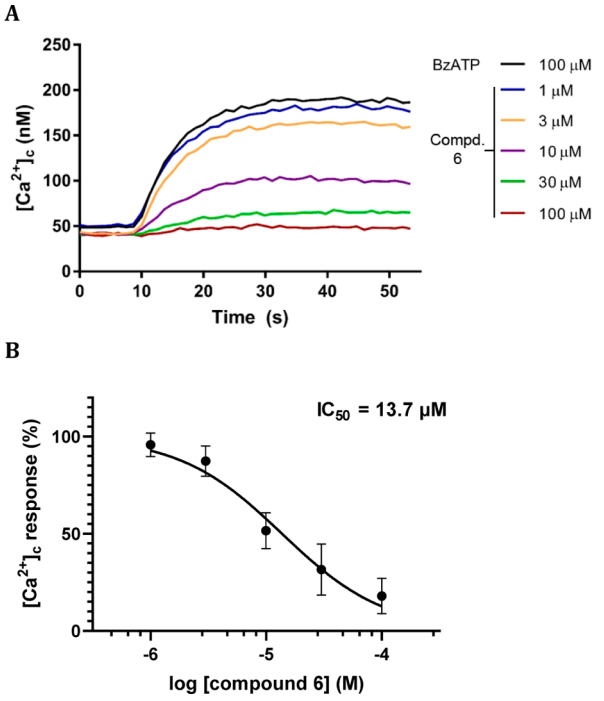

Figure 3. (A) Raw data representation of a FURA-2 intracellular Ca^{2+} dynamics experiment in the presence of increasing concentrations of compound **6** (ITH15004). The BzATP (100 μM) control response is shown in black. (B) Dose–response curve of **6** (ITH15004) in $[Ca^{2+}]_c$ dynamics. Dots represent the mean ± S.E.M. of three triplicates of three different cell cultures.

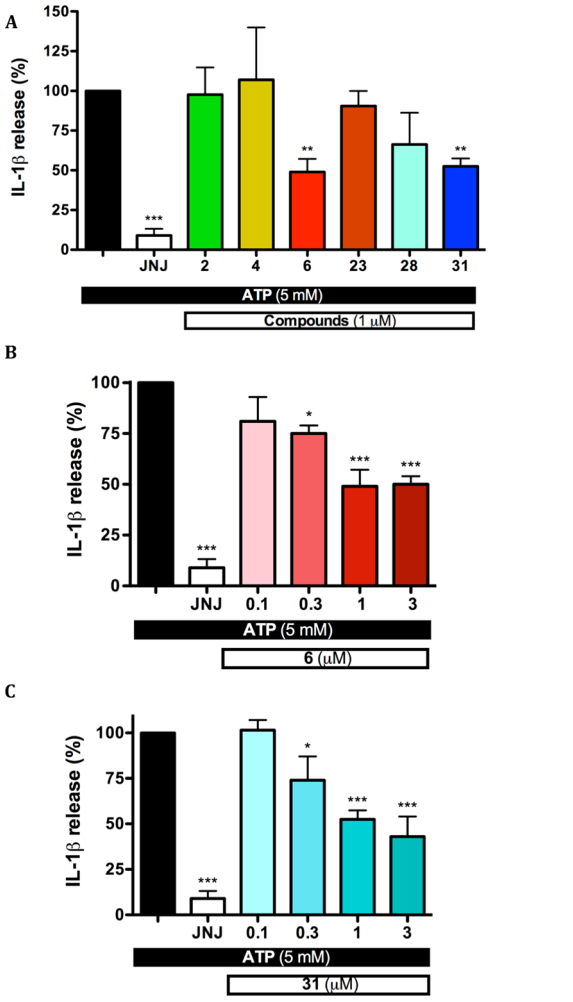

Figure 4. IL-1β release (%) from LPS-primed, ATP-stimulated MPMs in comparison to control (only ATP; black bar). (A) Cells were primed with LPS for 4 h and the compounds were added for 15 min at 1 μM. Cells were then stimulated with ATP for 30 min and the levels of IL-1β in medium were determined by ELISA. (B) Dose–response effect of compound **6**. (C) Dose–response effect of compound **31**. JNJ-47965567 (JNJ, tested at 0.1 μM) was used as the reference compound. Data are mean ± S.E.M. of triplicates of three different mice. *P < 0.05, **p < 0.01, ***p < 0.001 with respect to control (black bar).

receptor subtypes by TEVC in *X. laevis* oocytes (Figure 5). Compound **6** showed high selectivity for the human P2X7 against rat P2X1, P2X2, and P2X4 receptors. The selectivity is unlikely to be ascribable to species difference since compound **6** could still inhibit the rat P2X7, apparently with a higher potency (Figure S2, Supporting Information).

To direct the synthesis of the novel compounds toward BBB-permeable ligands, we had initially evaluated their physico-chemical properties, such as lipophilicity, number of hydrogen bonds donors and acceptors, and the molecular weight.

Later, we took advantage of the parallel artificial membrane permeability assay (PAMPA), which measures the molecular ability of compounds to cross a lipophilic membrane by passive diffusion. We selected the best inhibitory compounds among all the families. The majority of the tested compounds showed an elevated permeability that should guarantee their distribution within the CNS according to Di et al.[58] (Figure 6). Curiously, compound **16** has a lower permeability than the other structural analogues, although it bears an additional chlorine atom with respect to **6**. Replacement of chlorine with fluorine (**17**) leads to better permeability but not as much as when a hydrogen occupies the C2 position of the purine core. *N*-Alkylation and *N*-sulfonylation of theophylline induced a huge increase of BBB permeability as initially hypothesized (compounds **29**–**31**). Indeed, compound **31** showed a huge permeability rate. These derivatives, together with **6**, showed better permeability than the P2X7 antagonist JNJ-47965567 (JNJ).

Compounds **6** and **31** showed an interesting inhibitory activity on P2X7 and high permeability through lipid membranes. In order to predict whether they are able to endure in the CNS, we measured in addition their ability to stimulate the P-glycoprotein (Pgp) ATPase activity as potential substrates of this efflux pump, highly expressed in the BBB and responsible of expulsion of most of xenobiotics from the CNS. We also measured the effect of the well-known Pgp substrate verapamil and the P2X7 blocker JNJ-47965567 (JNJ), all of them tested at 10 μM. The Pgp substrate verapamil[59] up-regulated the ATPase activity of Pgp, measured as the variation in luminescence (R.L.U., Figure 7). Surprisingly, JNJ-47965567 strongly activated Pgp ATPase, too, meaning that it is likely to be an important substrate of the efflux pump. This was not reported yet in the literature, although *ex vivo* radioligand assays in rat brains demonstrated the capacity of JNJ-47965567 to endure in the CNS for at least 2 h,[60] with a continuous decrease in concentration during the time.[61] Unlike JNJ-47965567, compounds **6** and **31** did not affect Pgp ATPase activity in statistical significance (P = 0.09 and 0.16, respectively, Figure 7). Considering that human and rat P-

https://dx.doi.org/10.1021/acs.jmedchem.0c02145
J. Med. Chem. 2021, 64, 2272–2290

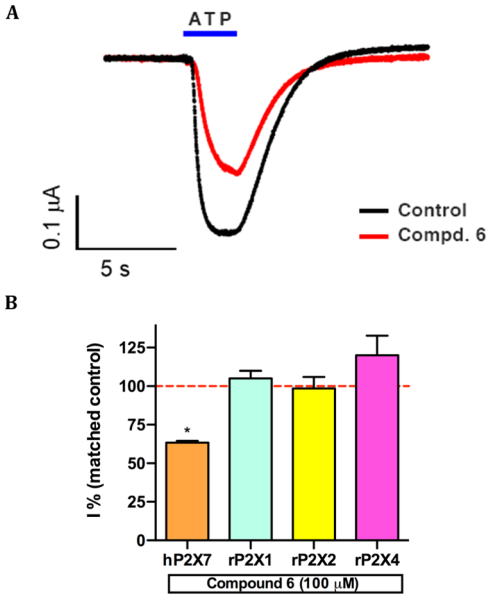

Figure 5. Evaluation of **6** by TEVC analysis. (A) Typical TEVC recording of ATP (300 μM, 2 s)-activated hP2X7 currents in the presence (red) and absence (black) of **6** at 100 μM. (B) Selective inhibition of hP2X7 but not of rP2X1, rP2X2, and rP2X4 by **6** at 100 μM. Data represent the mean ± S.E.M. of three oocytes from two different frogs, normalized to control current amplitude (marked as a horizontal dashed red line). *P < 0.001 compared to control.

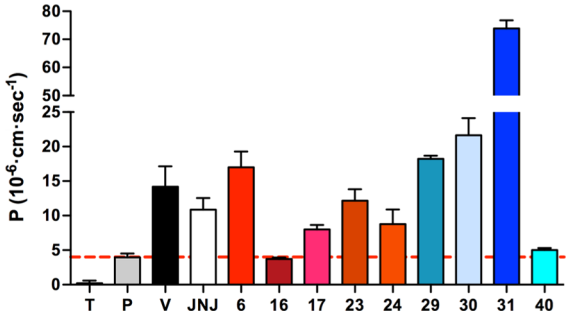

Figure 6. Permeability values of selected new compounds (reddish bars are purine analogues and bluish bars are xanthine analogues), measured by PAMPA experiments. Theophylline (T), piroxicam (P), and verapamil (V) were used as low-, middle-, and high-permeability standards, respectively. Their permeability constants in 10^{-6}·cm·s^{-1} are 0.12 (T), 2.5 (P), and 16 (V), similar to those described by Di et al.[58] The red line at $4{\cdot}10^{-6}$·cm·s^{-1} marks the theoretical threshold for guaranteeing CNS permeability. Data are presented as the mean ± S.E.M. of triplicates of three individual experiments performed in three different days.

glycoprotein activities are usually comparable,[62−64] our data suggest that our compounds could persist in the CNS similar to or even better than JNJ-47965567 despite its enhancing activity on the Pgp.

Computational Study. Finally, we wanted to predict the binding pose of compound **6**, being the most potent P2X7 ligand discovered in this work. Most of the antagonists developed so far act in a highly lipophilic allosteric binding pocket located between neighboring subunits in the extracellular domain (Figure 8). We ran docking experiments in this binding site using the model described by Bin Dayel and coworkers (Figure 8 and Video S1, Supporting Information).[11] The majority of the poses obtained placed the dichloroaryl

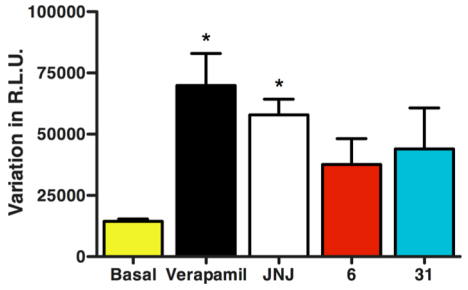

Figure 7. Effect of compounds **6** and **31** on Pgp ATPase activity compared with those of the Pgp substrate verapamil and the P2X7 blocker JNJ-47965567 (JNJ). Data are presented as the mean ± S.E.M. of triplicates of three individual experiments. *P < 0.05.

core deep into the pocket, interacting in a presumably $\pi-\pi$ stacking with phenylalanines 95 (F95), 103 (F103), and 293 (F293), as previously described for Calmidazolium.[11] Besides, all the antagonists crystallized in the pdP2X7 show their most lipophilic moiety in this vestibule.[9] The purine core, instead, is placed among tyrosine 295 (Y295) and 298 (Y298) as well as isoleucine 310 (I310) and methionine 105 (M105). The top area of the binding pocket is defined by the presence of phenylalanines 88 (F88) and 108 (F108), which suggests a halogen-aromatic interaction of the chlorine at C6 with these residues (Figure 8). This would explain why the compounds with polar groups at this position lose their activity. Moreover, the replacement of the chloride with a bulkier iodine at C6 reduces the potency, considering that the distance between halogen and F88/F108 is about 3.5 Å.[65] Noteworthily, many residues of this pocket have shown an essential contribution for receptor blockade in mutagenesis experiments.[9,11] Further investigation is needed to validate this *in silico* prediction and the potential involvement of these residues in ligand binding.

DISCUSSION

Despite efforts carried out by Big Pharma and Academia in the last decade, no P2X7 antagonists have reached clinical trials for the treatment of NDDs. Only JNJ-54175446 (Chart 1) drew attention for the potential treatment of a CNS disease, that is, major depression.[47,48] Indeed, the few candidates blocking P2X7 studied in clinical trials have focused on peripheral disorders.[49,50,66] This fact evidences the critical role that pharmacokinetics properties play in the selection of a drug candidate for NDDs besides high potency, selectivity, and an interspecies blocking effect. Most of the studies reported in literature to find a proper P2X7 antagonist for NDDs have focused only on pharmacological potency. When a head compound was selected, it commonly lacked an adequate pharmacokinetic profile to penetrate the CNS, forcing medicinal chemists to rethink all the design programs. Such is the case of the adamantine series, which showed a good P2X7 antagonist effect but a mediocre pharmacokinetic profile (for instance, $t_{1/2}$ = 0.22 h).[32]

In this work, we have paid attention to brain penetration, starting from the molecular design. First, we selected well-known scaffolds that are present in drugs with recognized CNS activity. Then, we corroborated that the target compounds fulfilled Lipinski's rule of five. These preliminary considerations guided us to synthesize and study the pharmacological scope of novel non-nucleotide purine derivatives as potential antagonists of P2X7. The purine scaffold of these novel compounds has been linked to a lipophilic group, that is, a substituted

https://dx.doi.org/10.1021/acs.jmedchem.0c02145
J. Med. Chem. 2021, 64, 2272−2290

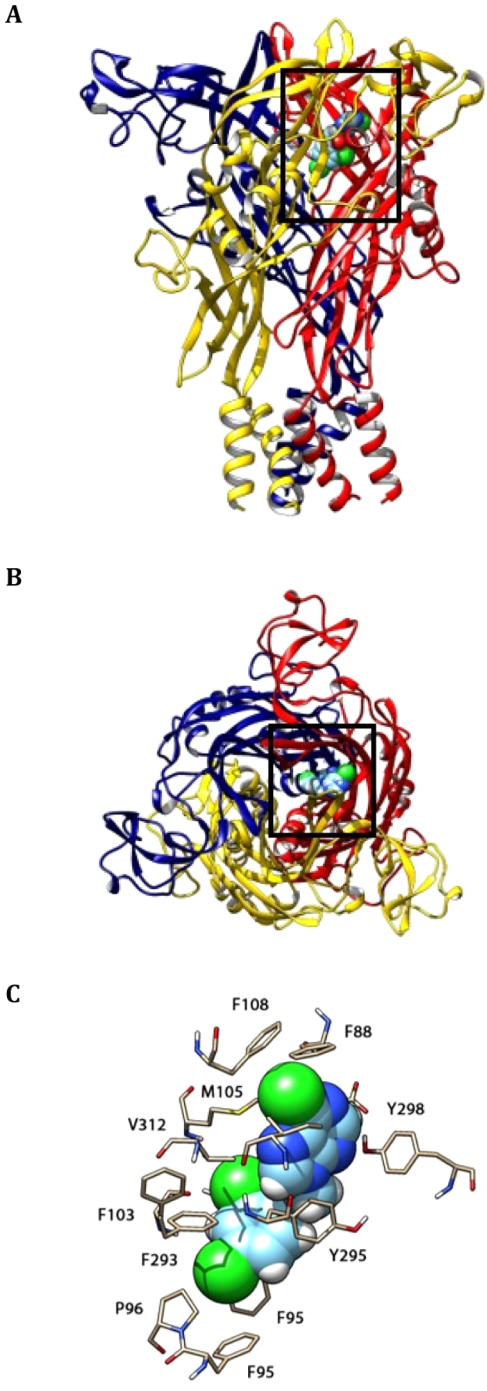

Figure 8. Lateral (A) and top (B) views of the ribbon-like representation of P2X7. The predicted binding site of compound **6** is indicated by the black frame. The residues defining the binding pocket are shown in C. The protein model was provided by Dayel et al.[11] with permission (crystal templates PDB IDs: 5U1U,5U1V, 5U1W, 5U1X, 5U1Y).

benzene, through a small spacer, namely, a carbonyl, a sulfonyl, and an ethanoyl moiety. All the data obtained through the pharmacological assays revealed that these features fit the structural properties necessary to inhibit the P2X7 but that more investigation is needed to fully define them. The most potent compound of our series, **6**, belongs to the family that possesses an ethanoyl group as the spacer. Only compound **31**, which bears a sulfonyl spacer and a theophylline core in its structure, showed a certain blockade. All its derivatives lose their inhibitory potency, and we consider that it might interact differently with P2X7 than purinylethanones. Compound **6** (2-(6-chloro-9*H*-purin-9-yl)-1-(2,4-dichlorophenyl)ethan-1-one), which we have named ITH15004, has a chlorine at C6, which can be replaced by other halogens such as iodine. However, this results in a decrease in potency. Substitution of the chlorine with a phenyl, like in **14**, might be permitted, but adding some polar substituent to increase compound solubility was an issue that led to contradictory data in this work. Also, the insertion of smaller halogens such as fluorine or non-voluminous alkyl chains at this position has not been tested yet as well as the effect of substituents at position 8 of the purine core. Small substituents at C2 are accepted with a decrease in potency, but a reduction in BBB-permeation is expected as happened for compound **16** in PAMPA. The removal of the chlorine at C2′ at the aryl group of the ethanoyl derivatives seems detrimental to blockade. This might be due to lipophilic interactions with V12 (Figure 8), one of the residues responsible for P2X7 inhibition with other antagonists.[9,11]

Compound **6** (ITH15004) elicits a concentration-dependent blockade of BzATP-evoked $[Ca^{2+}]_c$ transients in hP2X7-HEK293 cells, with an IC_{50} of 13.7 μM, and blocks by 63% at 10 μM the BzATP-induced YO-PRO-1 uptake in the same cellular model. At 100 μM, it also decreases by 47% the ATP (300 μM)-activated currents in *Xenopus laevis* oocytes expressing hP2X7. It was also shown to be P2X7-selective as it did not block rat P2X1, P2X2, or P2X4 but rat P2X7. Compound **6** also blocked mouse P2X7, halving the ATP-induced IL-1β release in LPS-primed MPMs, and exhibits a high lipophilic membrane permeability in the PAMPA, suggesting that it can permeate BBB and gain access to the brain.

Although the potency of compound **6** is in the micromolar range, its pharmacodynamic profile and BBB permeability suggest that this non-nucleotide purine derivative could serve as the starting point to design and synthesize new P2X7 blockers with moderate potency. This is relevant in the context of drug side effects and safety, which can be compromised with highly potent compounds that target P2X7 in the low nanomolar range. Moreover, it was observed that the complete removal of P2X7 in a mouse model of multiple sclerosis caused an exacerbation of the disease, probably due to P2X7-dependent changes in lymphocytic homeostasis,[67] which could also be affected by a chronic administration of a potent antagonist. Hence, we consider that a modulation of P2X7 by a chronic administration of a mild potent antagonist could potentially lead to better results. This could presume a point in favor for compounds **6** and **31** that confirmed the success of our chemical design, aimed at developing a P2X7 antagonist with improved pharmacokinetic profile and high BBB permeability rate. These features represent a fundamental issue that affects the development of agents targeting the CNS, such as the well-known P2X7 antagonist JNJ-47965567, which was never included in a clinical trial. Although it was demonstrated that it reaches the CNS,[60] we have observed for the first time that it also increases the Pgp ATPase activity, which could jeopardize its positive effects on CNS disorders. Pursuing this hypothesis is out of the scope of this work, but it underlines the necessity of a deeper focus on the pharmacokinetic parameters of potential new CNS drugs, as we have intended.

In conclusion, in this work, we have designed and synthesized a novel series of non-nucleotide purine derivatives

https://dx.doi.org/10.1021/acs.jmedchem.0c02145
J. Med. Chem. 2021, 64, 2272−2290

that show a certain effect as the P2X7 antagonist when an ethanoyl moiety is used as a spacer according to our designed model (Figure 1). Most of them have high lipophilicity, being adequate to target the CNS. ITH15004 was the best antagonist of the series and could be used as a tool for further *in vitro* and *in vivo* studies in neurodegenerative diseases where chronic administration and P2X7 modulation might be preferred. Future studies should be addressed to further explore the structure−activity relationships of this scaffold and evaluate other important features such as metabolism and CNS stability, without affecting its gained selectivity and good BBB permeability.

EXPERIMENTAL SECTION

General Procedures and Materials. Solvents and starting materials were used as supplied by Sigma-Aldrich, Merck KGaA (Madrid, Spain), unless otherwise indicated. Anhydrous and inert conditions for specific reactions were obtained using a Schlenk line (vacuum purges and Ar atm), and solvents were dried and freshly distilled over its corresponding adsorbent. Reactions were controlled by TLC (silica gel plates from Sigma-Aldrich, Merck KGaA). Detection was made with a UV light lamp at a wavelength of 254 nm. Flash normal-phase CC (CC) was carried out on an Isolera One (Biotage) using silica gel pre-packaged cartridges unless otherwise indicated. ^{1}H and ^{13}C NMR spectra were obtained in a spectrometer Bruker AVANCE 300 MHz and presented in ppm using the residual signal of the proton of the corresponding deuterated solvent as the internal standard. MS spectra were obtained in an ABSciex QSTAR spectrometer under the high-resolution configuration with electrospray as the ionization source. Melting points were obtained in an apparatus Stuart SMP-10 and are uncorrected. X-ray diffractions for selected compounds were performed using a Bruker D8 Kappa series apparatus, with radiation of graphite monochromated Mo Kα at a λ = 0.71073 Å. Full details of data collection and refinement have been described in the Supporting Information. CIF files have been deposited in the Cambridge Crystallographic Data Centre (CCDC) with the codes CCDC2023914 for the compound **19** X ray structure and CCDC2023913 for the compound **31** X ray structure. The tested compounds did not present potential PAINS activity according to screening in http://zinc15.docking.org/patterns/home.[68] The purity of the tested compounds was determined by elemental organic analysis on a station LECO-CHNS-932 or by HPLC-UV with a Varian Prostar analytical liquid chromatographer. Values of C, H, and N from elemental analyses data were within 0.4% of the calculated values for each final compound. The purity of all tested compounds is >95%.

Preparation of Synthetic Precursors. *6-Methoxypurine (**3**).* Metallic Na (200 mg, 9.1 mmol) was slowly added to MeOH (10 mL) in a flask under dry and inert conditions. After 30 min of stirring at rt, 6-chloropurine (350 mg, 2.3 mmol) was added. The mixture was heated to 60 °C and stirred for 2 h. The solvent was then evaporated under reduced pressure, and the crude was purified by filtration through a silica plug (gradient of methanol in CH_2Cl_2, 0/100 to 20/80). The filtrate was evaporated under vacuum obtaining a white powder that corresponded to **3** in quantitative yield. ^{1}H NMR (300 MHz, CD_3OD): δ 8.49 (s, 1H, H2), 8.27 (s, 1H, H8), 4.18 (s, 3H, CH_3).

*6-Chloro-9-(tetrahydro-2H-pyran-2-yl)purine (**7**).* 6-chloropurine (1.5 g, 9.7 mmol) and *p*-toluenesulfonic acid (PTSA, 33 mg, 0.19 mmol) were suspended in dry EtOAc (16 mL) in dry and inert conditions. The mixture was heated up to 50 °C, and 3,4-dihydropyran (DHP, 992 μL, 11 mmol) was added dropwise over 5 min. The reaction was stirred at 50 °C for 64 h. Then, aqueous ammonia was added until pH = 8. The mixture was diluted with EtOAc (10 mL) and water (10 mL). Then, the organic layer was separated, washed again with water and brine, dried over anhydrous Na_2SO_4, and filtered, and the solvent was evaporated under reduced pressure. The crude was purified by column chromatography (gradient of EtOAc in hexane, 18/82 to 100/0), giving compound **7** as a transparent oil that solidified upon standing (1.45 g, 62%). ^{1}H NMR (300 MHz, $CDCl_3$): δ 8.75 (s, 1H, H2), 8.34 (s, 1H, H8), 5.80 (dd, J = 10.2 Hz, 2.6 Hz, 1H, CHO), 4.20 (dd, J = 12.8, 3.0 Hz, 1H, CH_2O), 3.79 (td, J = 11.4, 3.1 Hz, 1H, CH_2O), 2.28−1.96 and 1.94−1.63 (2m, 6H, $(CH_2)_3CH_2O$).

*6-Phenyl-9-(tetrahydro-2H-pyran-2-yl)purine (**8**).* Intermediate **7** (138 mg, 0.58 mmol) was dissolved in freshly distilled toluene (6 mL) under dry and inert conditions. K_2CO_3 (116 mg, 0.84 mmol) and phenylboronic acid (102 mg, 0.84 mmol) were added, and the mixture was sonicated for 5 min under Ar bubbling. Tetrakis-(triphenylphosphine)palladium(0) (33 mg, 29 μmol) was added, and the reaction was refluxed overnight. After 15 h, the mixture was filtered, and the filtrate was concentrated under reduced pressure. The residue was purified by column chromatography (gradient of EtOAc in hexane, 18/82 to 100/0), obtaining **8** as a transparent oil that solidified upon standing (117 mg, 72%). ^{1}H NMR (300 MHz, acetone-d_6): δ 9.01−8.92 (m, 3H, H2′ and H2), 8.65 (s, 1H, H8), 7.63−7.52 (m, 3H, H3′, H4′), 5.90 (dd, J = 10.9, 2.4 Hz, 1H, CHO), 4.17−4.07 (m, 1H, CH_2O), 3.82 (td, J = 11.5, 3.1 Hz, 1H, CH_2O), 2.45−2.23, 2.20−2.08, 1.99−1.81, 1.79−1.60 (4m, 6H, $(CH_2)_3CH_2O$).

*6-Phenylpurine (**9**).* Intermediate **8** (117 mg, 0.42 mmol) was suspended in MeOH (4 mL). Acetyl chloride (8.3 μL, 0.12 mmol) was added, and the reaction was stirred at rt for 72 h. Then, the solvent was evaporated under reduced pressure, and the residue was washed with water (2 × 4 mL) and concentrated under vacuum, giving **9** as a white powder (69 mg, 84%). ^{1}H NMR (300 MHz, acetone-d_6): δ 9.04−8.94 (m, 2H, H2′), 8.93 (s, 1H, H2), 8.56 (s, 1H, H8), 7.65−7.52 (m, 3H, H3′, H4′).

*6-Chloro-2-fluoropurine (**10**).* Following the procedure described by Kim et al.,[69] 2-amino-6-chloropurine (100 mg, 0.59 mmol) was added to a solution of hydrofluoric acid in pyridine (70%, 1.5 mL) at −50 °C. The reaction was allowed to warm up to −30 °C, and *tert*-butyl nitrite (105 μL, 0.88 mmol) was added. The reaction was stirred at −30 °C for 20 min; then, it was quenched by adding water and ice (4 mL). The mixture was extracted with $CHCl_3$ (5 × 3 mL), and the organic fractions were washed with brine, dried over anhydrous Na_2SO_4, and filtered. After solvent evaporation under vacuum, the residue was purified by column chromatography (gradient of MeOH in DCM, 1/99 to 8/92), giving **10** as a white solid (43 mg, 42%). ^{1}H NMR (300 MHz, acetone-d_6): δ 8.60 (s, 1H, H8).

*2-Chloro-6-iodopurine (**11**).* Following the procedure described by Tobrman et al.,[70] 2,6-dichloropurine (100 mg, 0.53 mmol) was suspended in hydriodic acid (1 mL) at 0 °C. After 5 h of stirring, the reaction was diluted with water (2 mL) and NH_4OH was added until pH = 9. The mixture was decanted overnight, then filtered, washed with water (1 mL), and dried under vacuum, obtaining **11** as a yellowish powder (123 mg, 83%). ^{1}H NMR (300 MHz, acetone-d_6): δ 8.60 (s, 1H, H8).

*3-Chloro-1-(2,4-dichlorophenyl)propan-1-one (**21**).* $AlCl_3$ (252 mg, 1.9 mmol) was suspended in 1,3-dichlorobenzene (920 μL, 8 mmol) under dry and inert conditions. 3-Chloropropanoyl chloride (150 μL, 1.6 mmol) was added dropwise to the mixture, which was subsequently heated up to 60 °C and stirred for 4 h. Then, the mixture was cooled down to 0 °C and water (2 mL) was slowly added to quench the reaction. The mixture was extracted with EtOAc (3 × 3 mL), and the combined organic fraction was dried over anhydrous Na_2SO_4 and filtered, and the solvent was evaporated under reduced pressure. The residue was purified by CC (gradient of EtOAc in hexane, 2/98 to 20/80). After solvent evaporation under vacuum, intermediate **21** was obtained as a clear amber oil (307 mg, 82%). ^{1}H NMR (300 MHz, $CDCl_3$): δ 7.52 (d, J = 8.4 Hz, 1H, H6′), 7.46 (d, J = 2.0 Hz, H3′), 7.34 (dd, J = 8.4, 2.0 Hz, 1H, H5′), 3.88 (t, J = 6.6 Hz, 2H, CH_2CO), 3.76 (t, J = 6.6 Hz, 1H, CH_2CO), 3.44 (t, J = 6.5 Hz, 1H, CH_2Cl), 2.87 (t, J = 6.6 Hz, 1H, CH_2Cl).

2,6-Dichloropurin-9-ium Chloride. 2,6-Dichloropurine (100 mg, 0.53 mmol) was dissolved in a 3 M solution of HCl in cyclopentylmethylether (1 mL) under dry and inert conditions. The reaction was stirred at rt for 24 h and filtered. The resulting solid was

https://dx.doi.org/10.1021/acs.jmedchem.0c02145
J. Med. Chem. 2021, 64, 2272−2290

washed with diethyl ether (2 × 1 mL) and dried under vacuum, yielding **12** as a yellowish powder (84 mg, 70%). ^{1}H NMR (300 MHz, D_2O): δ 8.64 (s, 1H, H8).

*2-Chloro-9-methyl-1,9-dihydro-6H-purin-6-one (**39**).* Following the procedure described by Tumma et al.,[53] 2,6-dichloropurin-9-ium chloride (84 mg, 0.37 mmol) and basic alumina (38 mg) were suspended in MeOH (2 mL). The reaction was heated up to 70 °C and stirred for 24 h. The reaction was interrupted by solvent evaporation under reduced pressure, and the residue was purified by CC (gradient of MeOH in CH_2Cl_2, 2/98 to 16/84), yielding **39** as a white powder (26 mg, 38%). ^{1}H NMR (300 MHz, acetone-d_6): δ 8.32 (s, 1H, H8), 4.15 (s, 3H, CH_3).

General Procedure for the Synthesis of 2-Chlorobenzamides 2, 4, and 28. The 6-substituted purine or theobromine (1 equiv) was dissolved in freshly distilled THF (0.1 M) under dry and inert conditions. DMAP (0.05 equiv) and TEA (2 equiv) were injected, and the mixture was cooled down to 0 °C. 2-Chlorobenzoyl chloride (1 equiv) was added dropwise for 30 min, and the mixture was allowed to reach rt while stirring. After the reaction was completed (4−6 h for purines, 24 h at rt plus 24 h at 70 °C when theobromine was used as the substrate, TLC), the solvent was evaporated under reduced pressure, EtOAc (20 mL) and water (20 mL) were added to the crude, and the two layers were separated. The aqueous layer was extracted again with EtOAc (10 mL), and the combined organic fraction was washed with brine, dried over anhydrous Na_2SO_4, and filtered. The solvent was concentrated under reduced pressure, and the residue was purified by trituration in hexane several times to yield a pure product.

*(6-Chloro-9H-purin-9-yl)(2-Chlorophenyl)methanone (**2**).* 6-Chloropurine (227 mg, 1.5 mmol), 2-chlorobenzenesulfonyl chloride (186 μL, 1.5 mmol), DMAP (9 mg, 73.7 μmol), and TEA (410 μL, 3 mmol) in THF (15 mL) yielded **2** as a white powder (337 mg, 78%).^{1}H NMR (300 MHz, acetone-d_6): δ 9.02 (s, 1H, H2), 8.61 (s, 1H, H8), 7.88−7.52 (m, 4H, Ar). ^{13}C NMR (75.4 MHz, acetone-d_6): δ 164.0, 154.1, 152.1, 151.9, 145.5, 134.4, 133.7, 133.6, 132.3, 131.3, 131.0, 128.4. HRMS (ESI$^+$) mass calcd for $C_{12}H_6Cl_2N_4O$ (m/z) 292.9991 [M + H]$^+$; found, 292.9994. mp 133−135 °C. Anal. Calcd for $C_{12}H_6Cl_2N_4O$: C, 49.17; H, 2.06; N, 19.12. Found: C, 48.78; H, 2.40; N, 19.50.

*(2-Chlorophenyl)(6-methoxy-9H-purin-9-yl)methanone (**4**).* 6-Methoxypurine (**3**, 100 mg, 0.67 mmol), 2-chlorobenzenesulfonyl chloride (84.5 μL, 0.67 mmol), DMAP (4 mg, 33.3 μmol), and TEA (177 μL, 1.3 mmol) in THF (6.5 mL) yielded **4** as a white powder (102 mg, 53%). ^{1}H NMR (300 MHz, acetone-d_6): δ 8.74 (s, 1H, H2), 8.34 (s, 1H, H8), 7.80−7.52 (m, 4H, Ar), 4.15 (s, 3H, CH_3). ^{13}C NMR (75.4 MHz, acetone-d_6): δ 164.6, 162.3, 154.3, 152.3, 145.5, 142.1, 134.4, 134.1, 132.2, 131.1, 130.9, 128.4, 123.4, 54.8. HRMS (ESI$^+$) mass calcd for $C_{13}H_9ClN_4O_2$ (m/z) 311.0306 [M + Na]$^+$; found, 311.0302 [M + Na]$^+$. mp 169−171 °C. Anal. Calcd for $C_{13}H_9ClN_4O_2$: C, 54.09; H, 3.14; N, 19.41. Found: C, 54.00; H, 3.06; N, 18.95.

*1-(2-Chlorobenzoyl)-3,7-dimethyl-3,7-dihydro-1H-purine-2,6-dione (**28**).* Theobromine (3,7-dimethyl-3,7-dihydro-1*H*-purine-2,6-dione, 200 mg, 1.1 mmol), 2-chlorobenzoyl chloride (141 μL, 1.1 mmol), DMAP (7 mg, 57.3 μmol), and TEA (309 μL, 2.2 mmol) in THF (11 mL) yielded **28** as a white powder (196 mg, 55%). ^{1}H NMR (300 MHz, acetone-d_6): δ 8.01 (d, J = 7.9 Hz, 1H, H6′), 7.95 (s, 1H, H8), 7.70−7.60 (m, 2H, Ar), 7.48 (t, J = 7.4 Hz, 1H, Ar), 3.97 (s, 1H, N7CH_3), 3.47 (s, 1H, N3CH_3). ^{13}C NMR (75.4 MHz, acetone-d_6): δ 167.8, 154.6, 151.2, 150.8, 144.5, 135.5, 134.9, 133.6, 132.6, 132.6, 128.4, 108.1, 33.8. HRMS (ESI$^+$) mass calcd for $C_{14}H_{11}ClN_4O_3$ (m/z) 341.0411 [M + Na]$^+$; found, 341.0398. mp 182−183 °C. Anal. Calcd for $C_{14}H_{11}ClN_4O_3$: C, 52.76; H, 3.48; N, 17.58. Found: C, 52.66; H, 3.38; N, 17.56.

General Procedure for the Preparation of Purinyl/Xanthinyl-2,4-dichlorophenylethanones/propanones 6, 12−18, 20, 22, 29, and 30. Method A. The purine derivative used as the starting material (1 equiv) was dissolved in dry DMF (0.05 M) under dry and inert conditions and cooled down to 0 °C. NaH (60% dispersion in mineral oil, 1.2 equiv) was added, and the resulting mixture was stirred at rt for 30 min.[71] The corresponding 2-chloro-1-arylethan-1-one (1.5 equiv), dissolved in dry DMF (1 mL), was added dropwise at 0 °C over 45 min. The reaction was allowed to reach rt. After completion (15−40 h, TLC), the solvent was evaporated under vacuum and the residue was dissolved in EtOAc (30 mL) and water (20 mL). The layers were decanted, and the aqueous phase was extracted with EtOAc (2 × 10 mL). The combined organic fraction was washed with brine, dried over anhydrous Na_2SO_4, and filtered, and the solvent was evaporated under reduced pressure. The crude was purified by CC or trituration. Method B. The purine or xanthine derivative used as the starting material (1 equiv), 2-chloro-1-(2,4-dichlorophenyl)ethan-1-one (1.2 equiv), Bu_4NHSO_4 (0.05 equiv), and K_2CO_3 (1 equiv) were dissolved in dry DMF (0.2 M) under dry and inert conditions. The mixture was then heated up to 150 °C in a sealed tube. After completion (1−6 h, TLC), the solvent was evaporated under vacuum, and the residue was retrieved with CH_2Cl_2 (10 mL) and washed with water (2 × 4 mL). The organic fraction was dried over anhydrous Na_2SO_4 and filtered, and the solvent was evaporated under reduced pressure. The crude was eventually purified by CC.

*2-(6-Chloro-9H-purin-9-yl)-1-(2,4-dichlorophenyl)ethan-1-one (**6**).* Following method A, 6-chloropurine (100 mg, 0.65 mmol), 2-chloro-1-(2,4-dichlorophenyl)ethan-1-one (224 mg, 0.97 mmol), and NaH (60% dispersion in mineral oil, 31 mg, 776 μmol) in dry DMF (11 mL) yielded **6** as a white powder (50 mg, 45%) after purification by CC (gradient of EtOAc in hexane, 16/84 to 100/0). ^{1}H NMR (300 MHz, acetone-d_6): δ 8.71 (s, 1H, H2), 8.55 (s, 1H, H8), 8.03 (d, J = 8.4 Hz, 1H, H6′), 7.73 (d, J = 2.0 Hz, 1H, H3′), 7.63 (dd, J = 8.4, 2.0 Hz, 1H, H5′), 6.01 (s, 2H, CH_2). ^{13}C NMR (75.4 MHz, acetone-d_6): δ 193.4, 153.6, 152.8, 151.0, 148.3, 139.4, 134.9, 133.9, 132.7, 132.2, 131.8, 128.8, 53.2. HRMS (ESI$^+$) mass calcd for $C_{13}H_7Cl_3N_4O$ (m/z) 340.9758 [M + H]$^+$; found, 340.9759. mp 166−168 °C. Anal. Calcd for $C_{13}H_7Cl_3N_4O$: C, 45.71; H, 2.07; N, 16.40. Found: C, 45.69; H, 1.89; N, 16.50.

*2-(6-Chloro-9H-purin-9-yl)-1-(4-chlorophenyl)ethan-1-one (**12**).* Following method A, 6-chloropurine (100 mg, 0.65 mmol), 2-chloro-1-(4-chlorophenyl)ethan-1-one (183 mg, 0.97 mmol), and NaH (60% dispersion in mineral oil, 31 mg, 796 μmol) in dry DMF (10 mL) yielded **12** as a white powder (95 mg, 48%) after purification by CC (gradient of acetone in hexane, 10/90 to 80/20). ^{1}H NMR (300 MHz, acetone-d_6): δ 8.69 (s, 1H, H2), 8.53 (s, 1H, H8), 8.20 (d, J = 8.6 Hz, 2H, H2′), 7.68 (d, J = 8.6 Hz, 2H, H3′), 6.12 (s, 2H, CH_2). ^{13}C NMR (75.4 MHz, acetone-d_6): δ 191.6, 153.8, 152.7, 150.9, 148.5, 141.0, 134.0, 132.2, 131.0, 130.3, 50.8. HRMS (ESI$^+$) mass calcd for $C_{13}H_8Cl_2N_4O$ (m/z) 307.0147 [M + H]$^+$; found, 307.0161. mp 217 °C (dec.). Anal. Calcd for $C_{13}H_8Cl_2N_4O$: C, 50.84; H, 2.63; N, 18.24. Found: C, 50.77; H, 2.78; N, 18.26.

*2-(6-Chloro-9H-purin-9-yl)-1-(4-fluorophenyl)ethan-1-one (**13**).* Following method A, 6-chloropurine (100 mg, 0.65 mmol), 2-chloro-1-(4-fluorophenyl)ethan-1-one (167 mg, 0.97 mmol), and NaH (60% dispersion in mineral oil, 31 mg, 796 μmol) in dry DMF (10 mL) yielded **13** as a white powder (156 mg, 83%) after purification by CC (gradient of EtOAc in hexane, 12/88 to 100/0). ^{1}H NMR (300 MHz, acetone-d_6): δ 8.69 (s, 1H, H2), 8.54 (s, 1H, H8), 8.27 (ddd, J = 8.9, 4.6, 1.7 Hz, 2H, H2′), 7.46−7.34 (m, 2H, H3′), 6.12 (s, 2H, CH_2). ^{13}C NMR (75.4 MHz, acetone-d_6): δ 191.0, 167.1 (d, J = 253.3 Hz), 153.6, 152.5, 150.8, 148.4, 132.1 (d, J = 9.8 Hz), 131.9, 131.9, 116.9 (d, J = 21.9 Hz), 50.6. HRMS (ESI$^+$) mass calcd for $C_{13}H_8ClFN_4O$ (m/z) 291.0443 [M + H]$^+$; found, 291.0454. mp 162−165 °C. Anal. Calcd for $C_{13}H_8ClFN_4O$: C, 53.72; H, 2.77; N, 19.27. Found: C, 53.86; H, 2.93; N, 19.37.

*1-(2,4-Dichlorophenyl)-2-(6-phenyl-9H-purin-9-yl)ethan-1-one (**14**).* Following method A, 6-phenylpurine (**9**, 55 mg, 0.28 mmol), 2-chloro-1-(2,4-dichlorophenyl)ethan-1-one (**5**, 97 mg, 0.42 mmol), and NaH (60% dispersion in mineral oil, 13 mg, 336 μmol) in dry DMF (7 mL) yielded **14** as a yellowish powder (55 mg, 41%) after purification by CC (gradient of EtOAc in hexane, 15/85 to 100/0). ^{1}H NMR (300 MHz, acetone-d_6): δ 9.04−8.98 (m, 2H, C6Ar), 8.94 (s, 1H, H2), 8.56 (s, 1H, H8), 8.04 (d, J = 8.4 Hz, 1H, H6′), 7.73 (d, J = 2.0 Hz, 1H, H3′), 7.68−7.51 (m, 4H, C6Ar, H5′), 5.99 (s, 2H,

https://dx.doi.org/10.1021/acs.jmedchem.0c02145
J. Med. Chem. 2021, 64, 2272−2290

CH_2). ^{13}C NMR (75.4 MHz, acetone-d_6): δ 194.0, 154.4, 154.1, 153.1, 147.3, 139.3, 137.0, 135.2, 133.8, 132.6, 131.9, 131.7, 131.5, 130.8, 129.4, 128.8, 52.7. HRMS (ESI^+) mass calcd for $C_{19}H_{12}Cl_2N_4O$ (m/z) 383.0460 $[M + H]^+$; found, 383.0465. mp 160−162 °C. Anal. Calcd for $C_{19}H_{12}Cl_2N_4O$: C, 59.55; H, 3.16; N, 14.62. Found: C, 59.58; H, 3.43; N, 14.48.

*1-(2,4-Dichlorophenyl)-2-(6-methoxy-9H-purin-9-yl)ethan-1-one (**15**).* Following method A, 6-methoxypurine (**3**, 100 mg, 0.67 mmol), 2-chloro-1-(2,4-dichlorophenyl)ethan-1-one (**5**, 223 mg, 1.0 mmol), and NaH (60% dispersion in mineral oil, 32 mg, 799 μmol) in dry DMF (11 mL) yielded **15** as a yellowish powder (53 mg, 24%) after purification by CC (gradient of acetone in hexane, 12/88 to 80/20). ^1H NMR (300 MHz, acetone-d_6): δ 8.47 (s, 1H, H2), 8.25 (s, 1H, H8), 7.99 (d, J = 8.4 Hz, 1H, H6′), 7.71 (d, J = 2.1 Hz, 1H, H3′), 7.61 (dd, J = 8.3, 2.2 Hz, 1H, H5′), 5.89 (s, 2H, CH_2), 4.15 (s, 3H, CH_3). ^{13}C NMR (75.4 MHz, acetone-d_6): δ 194.0, 161.9, 153.7, 152.7, 144.7, 139.1, 135.2, 133.6, 132.5, 131.6, 128.7, 121.8, 54.4, 52.8. HRMS (ESI^+) mass calcd for $C_{14}H_{10}Cl_2N_4O_2$ (m/z) 337.0253 $[M + H]^+$; found, 337.0256. mp 158 °C (dec). Anal. Calcd for $C_{14}H_{10}Cl_2N_4O_2$: C, 49.87; H, 2.99; N, 16.62. Found: C, 50.01; H, 3.11; N, 16.38.

*2-(2,6-Dichloro-9H-purin-9-yl)-1-(2,4-dichlorophenyl)ethan-1-one (**16**).* Following method A, 2,6-dichloropurine (100 mg, 0.53 mmol), 2-chloro-1-(2,4-dichlorophenyl)ethan-1-one (**5**, 183 mg, 0.79 mmol), and NaH (60% dispersion in mineral oil, 25 mg, 635 μmol) in dry DMF (18 mL) yielded **16** as a yellowish powder (65 mg, 40%) after purification by CC (gradient of EtOAc in hexane, 12/88 to 100/0) and trituration in diethyl ether. ^1H NMR (300 MHz, acetone-d_6): δ 8.57 (s, 1H, H8), 8.05 (d, J = 8.4 Hz, 1H, H6′), 7.73 (d, J = 2.0 Hz, 1H, H3′), 7.63 (dd, J = 8.4, 2.0 Hz, 1H, H3′), 6.01 (s, 2H, CH_2). ^{13}C NMR (75.4 MHz, acetone-d_6): δ 192.9, 155.2, 153.1, 151.7, 149.3, 139.6, 134.6, 134.1, 132.9, 131.9, 131.6, 128.9, 53.4. HRMS (ESI^+) mass calcd for $C_{13}H_6Cl_4N_4O$ (m/z) 374.9368 $[M + H]^+$; found, 374.9374. Mp 136−138 °C. Anal. calcd for $C_{13}H_6Cl_4N_4O$: C, 41.53; H, 1.61; N, 14.90. Found: C, 41.78; H, 1.93; N, 14.81.

*2-(6-Chloro-2-fluoro-9H-purin-9-yl)-1-(2,4-dichlorophenyl)-ethan-1-one (**17**).* Following method A, 6-chloro-2-fluoropurine (**10**, 42 mg, 0.24 mmol), 2-chloro-1-(2,4-dichlorophenyl)ethan-1-one (**5**, 82 mg, 0.36 mmol), and NaH (60% dispersion in mineral oil, 15 mg, 365 μmol) in dry DMF (4 mL) yielded **17** as a yellow oil (34 mg, 39%) after purification by CC (gradient of acetone in hexane, 6/94 to 50/50). ^1H NMR (300 MHz, acetone-d_6): δ 8.55 (s, 1H, H8), 8.04 (d, J = 8.4 Hz, 1H, H6′), 7.73 (d, J = 2.0 Hz, 1H, H3′), 7.63 (dd, J = 8.4, 2.0 Hz, 1H, H5′), 5.98 (s, 2H, CH_2). ^{13}C NMR (75.4 MHz, acetone-d_6): δ 191.9, 157.9 (d, J = 214.9 Hz), 154.7 (d, J = 17.3 Hz), 151.4 (d, J = 18.1 Hz), 148.2 (d, J = 3.0 Hz), 138.5, 133.6, 133.0, 131.8, 130.8, 130.1 (d, J = 6.8 Hz), 127.8, 52.3. HRMS (ESI^+) mass calcd for $C_{13}H_6Cl_3FN_4O$ (m/z) 358.9663 $[M + H]^+$; found, 358.9657. mp 134 °C. HPLC-UV (λ = 260 nm): purity 98%.

*2-(2-Chloro-6-iodo-9H-purin-9-yl)-1-(2,4-dichlorophenyl)ethan-1-one (**18**).* Following method A, 2-chloro-6-iodopurine (**11**, 69 mg, 0.25 mmol), 2-chloro-1-(2,4-dichlorophenyl)ethan-1-one (**5**, 85 mg, 0.37 mmol), and NaH (60% dispersion in mineral oil, 15 mg, 369 μmol) in dry DMF (4 mL) yielded **18** as a yellowish powder (30 mg, 28%) after purification by trituration in diethyl ether. ^1H NMR (300 MHz, acetone-d_6): δ 8.55 (s, 1H, H8), 8.04 (d, J = 8.4 Hz, 1H, H6′), 7.73 (d, J = 2.1 Hz, 1H, H3′), 7.63 (dd, J = 8.4, 2.1 Hz, 1H, H5′), 5.97 (s, 2H, CH_2). ^{13}C NMR (75.4 MHz, acetone-d_6): δ 191.9, 151.7, 150.1, 147.5, 138.5, 138.0, 133.5, 133.0, 131.8, 130.8, 127.8, 121.7, 52.2. HRMS (ESI^+) mass calcd for $C_{13}H_6Cl_3IN_4O$ (m/z) 466.8724 $[M + H]^+$; found, 466.8721. mp 214−215 °C (dec). HPLC-UV (λ = 284 nm): purity 100%.

*2-(2-Amino-6-chloro-9H-purin-9-yl)-1-(2,4-dichlorophenyl)-ethan-1-one (**20**).* Following method B, 6-chloropurin-2-amine (100 mg, 0.53 mmol), 2-chloro-1-(2,4-dichlorophenyl)ethan-1-one (**5**, 145 mg, 0.65 mmol), Bu_4NHSO_4 (10 mg, 29 μmol), and K_2CO_3 (81 mg, 0.59 mmol) in dry DMF (3 mL) yielded **20** as a brown powder (15 mg, 10%) after 30 h of reaction time at 80 °C and purification by CC (gradient of MeOH in CH_2Cl_2, 1/99 to 8/92) and trituration in cold EtOAc. ^1H NMR (300 MHz, acetone-d_6): δ 8.03 (s, 1H, H8), 7.96 (d, J = 8.4 Hz, 1H, H6′), 7.70 (d, J = 2.0 Hz, 1H, H3′), 7.60 (dd, J = 8.4, 2.0 Hz, 1H, H5′), 6.17 (br, 2H, NH_2), 5.69 (s, 2H, CH_2). ^{13}C NMR (75.4 MHz, acetone-d_6): δ 194.1, 161.1, 155.6, 151.3, 144.3, 139.2, 135.3, 133.7, 132.6, 131.6, 128.8, 125.1, 52.6. HRMS (ESI^+) mass calcd for $C_{13}H_8Cl_3N_5O$ (m/z) 355.9867 $[M + H]^+$; found, 355.9873. mp 208−209 °C (dec). HPLC-UV (λ = 306 nm), purity 99%.

*3-(6-Chloro-9H-purin-9-yl)-1-(2,4-dichlorophenyl)propan-1-one (**22**).* Following method A, 6-chloropurine (75 mg, 0.49 mmol), intermediate **21** (174 mg, 0.73 mmol), and NaH (60% dispersion in mineral oil, 23 mg, 586 μmol) in dry DMF (10 mL) yielded **22** as a white powder (40 mg, 23%) after purification by CC (gradient of EtOAc in hexane, 20/80 to 100/0). ^1H NMR (300 MHz, acetone-d_6): δ 8.70 (s, 1H, H2), 8.55 (s, 1H, H8), 7.72 (d, J = 8.4 Hz, 1H, H6′), 7.58 (d, J = 2.1 Hz, 1H, H3′), 7.48 (dd, J = 8.4, 2.0 Hz, 1H, H5′), 4.80 (t, J = 6.3 Hz, 2H, NCH_2), 3.81 (t, J = 6.3 Hz, 2H, CH_2CO). ^{13}C NMR (75.4 MHz, acetone-d_6): δ 198.3, 152.3, 151.4, 149.7, 147.2, 137.2, 136.6, 131.9, 131.5, 130.9, 130.3, 127.5, 41.3, 39.1. HRMS (ESI^+) mass calcd for $C_{14}H_9Cl_3N_4O$ (m/z) 354.9914 $[M + H]^+$; found, 354.9919. mp 140 °C (dec). HPLC-UV (λ = 256 nm), purity 99%.

*1-[2-(2,4-Dichlorophenyl)-2-oxoethyl]-3,7-dimethyl-3,7-dihydro-1H-purine-2,6-dione (**29**).* Following method B, theobromine (3,7-dimethyl-3,7-dihydro-1*H*-purine-2,6-dione, 70 mg, 0.39 mmol), 2-chloro-1-(2,4-dichlorophenyl)ethan-1-one (**5**, 104 mg, 0.47 mmol), Bu_4NHSO_4 (7 mg, 19 μmol), and K_2CO_3 (54 mg, 0.39 mmol) in dry DMF (2 mL) yielded **29** as a brown powder (36 mg, 25%) after purification by CC (gradient of MeOH in EtOAc, 0/100 to 4/96) and trituration in diethyl ether. ^1H NMR (300 MHz, acetone-d_6): δ 7.89 (s, 1H, H8), 7.86 (d, J = 8.3 Hz, 2H, H6′), 7.67 (d, J = 2.0 Hz, 1H, H3′), 7.58 (dd, J = 8.4, 2.0 Hz, 1H, H5′), 5.28 (s, 2H, CH_2), 3.99 (s, 3H, N7CH_3), 3.51 (s, 3H, N3CH_3). ^{13}C NMR (75.4 MHz, acetone-d_6): δ 195.4, 155.3 152.0, 150.2, 143.9, 138.4, 136.6, 133.1, 132.1, 131.3, 128.6, 50.2, 33.8. HRMS (ESI^+) mass calcd for $C_{15}H_{12}Cl_2N_4O_3$ (m/z) 367.0359 $[M + H]^+$; found, 367.0367. mp 196 °C (dec.). Anal. Calcd for $C_{15}H_{12}Cl_2N_4O_3$: C, 49.07; H, 3.29; N, 15.26. Found: C, 49.05; H, 3.39; N, 15.19.

*9-[2-(2,4-Dichlorophenyl)-2-oxoethyl]-1,3-dimethyl-3,7-dihydro-1H-purine-2,6-dione (**30**).* Following method B, theophylline (1,3-dimethyl-3,9-dihydro-1*H*-purine-2,6-dione, 70 mg, 0.39 mmol), 2-chloro-1-(2,4-dichlorophenyl)ethan-1-one (**5**, 104 mg, 0.47 mmol), Bu_4NHSO_4 (7 mg, 19 μmol), and K_2CO_3 (54 mg, 0.39 mmol) in dry DMF (2 mL) yielded **30** as a white powder (65 mg, 46%) after purification by CC (gradient of MeOH in EtOAc, 1/99 to 10/90) and trituration in diethyl ether. ^1H NMR (300 MHz, acetone-d_6): δ 8.04−7.94 (m, 2H, H8, H6′), 7.69 (d, J = 2.1 Hz, 1H, H3′), 7.62 (dd, J = 8.4, 2.1 Hz, 1H, H5′), 5.87 (s, 2H, CH_2), 3.53 (s, 3H, N3CH_3), 3.26 (s, 3H, N1CH_3). ^{13}C NMR (75.4 MHz, acetone-d_6): δ 194.1, 156.2, 152.4, 149.7, 144.0, 139.1, 135.6, 133.5, 132.7, 131.5, 128.8, 107.7, 55.8, 28.0. HRMS (ESI^+) mass calcd for $C_{15}H_{12}Cl_2N_4O_3$ (m/z) 367.0359 $[M + H]^+$; found, 367.0368. mp 198−199 °C. HPLC-UV (λ = 260 nm), purity 97%.

*2-[2-Chloro-6-(methylamino)-9H-purin-9-yl]-1-(2,4-dichlorophenyl)ethan-1-one (**19**).* 2-Chloro-*N*-methylpurin-6-amine (60 mg, 0.33 mmol), Bu_4NHSO_4 (5.5 mg, 16 μmol), and KOH (18 mg, 0.33 mmol) were suspended in dry DMF (2 mL) under dry and inert conditions. 2-Chloro-1-(2,4-dichlorophenyl)ethan-1-one (**5**, 80 mg, 0.36 mmol) was dissolved in dry DMF (0.5 mL) and added dropwise to the reaction at 0 °C over 45 min. The reaction was stirred at rt for 26 h and then it was diluted with cold water (6 mL) and EtOAc (7 mL). The mixture was stirred for 30 min after which the two layers were separated. The aqueous fraction was extracted with EtOAc (3 × 3 mL), and the combined organic layer was washed with brine, dried over anhydrous Na_2SO_4, filtered, and evaporated under reduced pressure. The crude was purified by CC (gradient of EtOAc in hexane, 18/82 to 100/0). After solvent evaporation, the solid was triturated with diethyl ether, furnishing **19** as a white solid (27 mg, 22%). The compound was recrystallized in EtOAc by slow evaporation to obtain crystals for X-ray diffraction (experimental details in the Supporting Information). ^1H NMR (300 MHz, acetone-

https://dx.doi.org/10.1021/acs.jmedchem.0c02145
J. Med. Chem. 2021, 64, 2272−2290

d_6): δ 8.02 (s, 1H, H8), 7.98 (d, J = 8.4 Hz, 1H, H6′), 7.70 (d, J = 2.1 Hz, 1H, H3′), 7.61 (dd, J = 8.4, 2.1 Hz, 1H, H5′), 7.24 (br s, 1H, NH), 5.75 (s, 2H, CH_2), 3.12 (s, 3H, CH_3). ^{13}C NMR (75.4 MHz, acetone-d_6): δ 193.9, 157.1, 154.3, 142.4, 139.1, 135.1, 133.6, 132.5, 131.5, 128.6, 119.2, 52.5, 27.7. HRMS (ESI$^+$) mass calcd for $C_{14}H_{10}Cl_3N_5O$ (m/z) 370.0023 [M + H]$^+$; found, 370.0041. mp 213 °C (dec). Anal. Calcd for $C_{14}H_{10}Cl_3N_5O·H_2O$: C, 43.27; H, 3.11; N, 18.02. Found: C, 43.33; H, 2.80; N, 17.99.

General Procedure for the Synthesis of Sulfonamides 23−27 and 31−38. Method A. The purine derivative (1 equiv) was dissolved in freshly distilled CH_2Cl_2 and THF (1:1, 0.1 M) under dry and inert conditions. DMAP (0.2 equiv) and TEA (2 equiv) were added, and the mixture was cooled down to 0 °C. 2-Chlorobenzenesulfonyl chloride (2 equiv) was added dropwise for 30 min. The mixture was stirred at rt, and after completion (2−4 h, TLC), the solvent was removed under reduced pressure. The crude was dissolved in EtOAc (30 mL) and water (20 mL), and the two layers were separated. The aqueous layer was extracted again with EtOAc (10 mL), and the combined organic fraction was washed with brine, dried over anhydrous Na_2SO_4, and filtered. The solvent was evaporated under reduced pressure and the residue purified by CC or trituration to yield the pure product. Method B. Theophylline (1,3-dimethyl-3,9-dihydro-1*H*-purine-2,6-dione, 1 equiv) was suspended in freshly distilled THF (0.05 M) in dry and inert conditions. The mixture was cooled down to 0 °C and NaH (60% dispersion in mineral oil, 1.2 equiv) was added, allowing the reaction to stir at rt for 30 min. The corresponding arylsulfonyl chloride derivative (1.2 equiv) was dissolved in dry THF (1 mL) and added to the reaction dropwise at 0 °C for 15 min. The reaction was stirred at rt, and after completion (4−48 h, TLC), the solvent was evaporated under reduced pressure. The residue was dissolved in EtOAc (30 mL) and water (30 mL). The layers were separated, and the aqueous layer was extracted once again with EtOAc (20 mL). The combined organic fraction was washed with brine, dried over anhydrous Na_2SO_4, and filtered. The solvent was evaporated under reduced pressure, and the residue was purified by CC to yield the pure product.

*6-Chloro-9-[(2-chlorophenyl)sulfonyl]-9H-Purine (**23**).* Following method A, 6-chloropurine (100 mg, 0.65 mmol), 2-chlorobenzenesulfonyl chloride (176 μL, 1.3 mmol), DMAP (16 mg, 129 μmol), and TEA (180 μL, 1.3 mmol) in CH_2Cl_2/THF (6.5 mL) yielded **23** as a white powder (165 mg, 77%) after trituration with cold MeOH. ^{1}H NMR (300 MHz, acetone-d_6): δ 9.05 (s, 1H, H2), 8.70 (s, 1H, H8), 8.60 (dd, J = 7.9, 1.9 Hz, 1H, H6′), 7.93−7.74 (m, 2H, H4′, H5′), 7.67 (dd, J = 7.9, 1.5 Hz, 1H, H3′). ^{13}C NMR (75.4 MHz, acetone-d_6): δ 154.2, 152.1, 151.4, 145.5, 138.3, 134.6, 134.5, 133.4, 133.1, 129.1. HRMS (ESI$^+$) mass calcd for $C_{11}H_6Cl_2N_4O_2S$ (m/z) 328.9661 [M + H]$^+$; found, 328.9663. mp 172 °C (dec). Anal. Calcd for $C_{11}H_6Cl_2N_4O_2S$: C, 40.14; H, 1.84; N, 17.02; S, 9.74. Found: C, 40.12; H, 2.06; N, 16.66; S, 9.75.

*2,6-Dichloro-9-[(2-chlorophenyl)sulfonyl]-9H-purine (**24**).* Following method A, 2,6-dichloropurine (100 mg, 0.53 mmol), 2-chlorobenzenesulfonyl chloride (144 μL, 1.1 mmol), DMAP (13 mg, 106 μmol), and TEA (147 μL, 1.1 mmol) in CH_2Cl_2/THF (5.3 mL) yielded **24** as a white powder (90 mg, 47%) after purification by CC (gradient of EtOAc in hexane, 0/100 to 50/50). ^{1}H NMR (300 MHz, acetone-d_6): δ 9.07 (s, 1H, H8), 8.58 (dd, J = 8.0, 1.9 Hz, 1H, H6′), 7.95−7.75 (m, 2H, H4′, H5′), 7.70 (dd, J = 7.9, 1.2 Hz, 1H, H3′). ^{13}C NMR (75.4 MHz, acetone-d_6): δ 154.7, 153.0, 152.8, 146.2, 138.6, 134.8, 134.4, 133.7, 133.6, 132.9, 129.3. HRMS (ESI$^+$) mass calcd for $C_{11}H_5Cl_3N_4O_2S$ (m/z) 362.9271 [M + H]$^+$; found, 362.9285. Mp 156 °C (dec). Anal. Calcd for $C_{11}H_5Cl_3N_4O_2S$: C, 36.34; H, 1.39; N, 15.41; S, 8.82. Found: C, 36.06; H, 1.58; N, 15.20; S, 9.14.

*9-[(2-Chlorophenyl)sulfonyl]-6-methoxy-9H-purine (**25**).* Following method A, 6-methoxypurine (**3**, 90 mg, 0.60 mmol), 2-chlorobenzenesulfonyl chloride (163 μL, 1.2 mmol), DMAP (15 mg, 120 μmol), and TEA (167 μL, 1.2 mmol) in CH_2Cl_2/THF (6 mL) yielded **25** as a white powder (72 mg, 37%) after purification by trituration with cold MeOH. ^{1}H NMR (300 MHz, acetone-d_6): δ 8.76 (s, 1H, H2), 8.57 (dd, J = 7.9, 1.9 Hz, 1H, H6′), 8.43 (s, 1H, H8), 7.85−7.77 (m, 2H, H4′, H5′), 7.66 (dd, J = 7.8, 1.5 Hz, 1H, H3′), 4.13 (s, 3H, CH_3). ^{13}C NMR (75.4 MHz, acetone-d_6): δ 162.2, 154.5, 151.5, 142.3, 138.0, 134.9, 134.6, 133.2, 133.1, 129.0, 122.6, 54.9. HRMS (ESI$^+$) mass calcd for $C_{12}H_9ClN_4O_3S$ (m/z) 346.9976 [M + Na]$^+$; found, 346.9980. mp 158 °C (dec). Anal. Calcd for $C_{12}H_9ClN_4O_3S$: C, 44.38; H, 2.79; N, 17.25; S, 9.87. Found: C, 44.48; H, 2.99; N, 16.94; S, 9.93.

*6-Chloro-9-[(2-chlorophenyl)sulfonyl]-9H-purin-2-amine (**26**).* Following method A, 6-chloropurin-2-amine (100 mg, 0.59 mmol), 2-chlorobenzenesulfonyl chloride (161 μL, 1.2 mmol), DMAP (14 mg, 118 μmol), and TEA (164 μL, 1.2 mmol) in CH_2Cl_2/THF (6 mL) yielded **26** as a white powder (102 mg, 50%) after purification by CC (gradient of EtOAc in hexane, 12/88 to 85/15). ^{1}H NMR (300 MHz, acetone-d_6): δ 8.51−8.42 (m, 2H, H8, H6′), 7.84 (td, J = 7.7, 1.7 Hz, 1H, H5′), 7.77−7.62 (m, 2H, H3′, H4′), 6.52 (br s, 2H, NH_2). ^{13}C NMR (75.4 MHz, $CDCl_3$): δ 161.8, 153.5, 152.5, 140.8, 137.9, 135.0, 134.7, 133.3, 133.2, 128.9, 125.1. HRMS (ESI$^+$) mass calcd for $C_{11}H_7Cl_2N_5O_2S$ (m/z) 343.9770 [M + H]$^+$ and 365.9589 [M + Na]$^+$; found, 343.9765 and 365.9573. mp 200 °C (dec). Anal. Calcd for $C_{11}H_7Cl_2N_5O_2S$: C, 38.39; H, 2.05; N, 20.35; S, 9.32. Found: C, 38.66; H, 2.37; N, 19.91; S, 9.23.

*2-Chloro-9-[(2-chlorophenyl)sulfonyl]-N-methyl-9H-purin-6-amine (**27**).* Following method A, 2-chloro-*N*-methylpurin-6-amine (100 mg, 0.54 mmol), 2-chlorobenzenesulfonyl chloride (148 μL, 1.1 mmol), DMAP (13 mg, 118 μmol), and TEA (152 μL, 1.1 mmol) in CH_2Cl_2/THF (6 mL) yielded **27** as a white powder (94 mg, 48%) after purification by CC (gradient of EtOAc in hexane, 12/88 to 100/0). ^{1}H NMR (300 MHz, acetone-d_6): δ 8.55−8.46 (m, 2H, H8, H6′), 7.91−7.71 (m, 2H, H5′, H4′), 7.67 (dd, J = 7.9, 1.4 Hz, 1H, H3′), 7.55 (br s, 1H, NH), 3.07 (d, J = 4.4 Hz, 3H, CH_3). ^{13}C NMR (75.4 MHz, DMSO-d_6): δ 155.4, 154.9, 147.9, 139.6, 137.4, 133.2, 133.1, 132.4, 131.3, 126.2, 118.4, 27.2. HRMS (ESI$^+$) mass calcd for $C_{12}H_9Cl_2N_5O_2S$ (m/z) 357.9926 [M + H]$^+$; found, 357.9932. mp 235 °C (dec). HPLC-UV (λ = 260 nm), purity 96%.

*7-[(2-Chlorophenyl)sulfonyl]-1,3-dimethyl-3,7-dihydro-1H-purine-2,6-dione (**31**).* Following method B, theophylline (60 mg, 0.33 mmol), 2-chlorobenzenesulfonyl chloride (55 μL, 0.40 mmol), and NaH (60% dispersion in mineral oil, 16 mg, 0.4 mmol) in THF (5.5 mL) yielded **31** as a white powder (82 mg, 69%) after purification by CC (gradient of EtOAc in hexane, 12/88 to 100/0). The compound was recrystallized in CH_2Cl_2 and acetone by slow evaporation to obtain crystals for X-ray diffraction (Supporting Information). ^{1}H NMR (300 MHz, acetone-d_6): δ 8.70 (s, 1H, H8), 8.60 (dd, J = 8.1, 1.7 Hz, 1H, H6′), 7.88−7.84, 7.76−7.66 (2m, 3H, Ar), 3.52 (s, 3H, N3CH_3), 3.16 (s, 3H, N1CH_3). ^{13}C NMR (75.4 MHz, $CDCl_3$): δ 153.6, 152.0, 151.8, 151.3, 145.4, 138.0, 136.1, 134.6, 133.3, 132.8, 128.6, 28.5. HRMS (ESI$^+$) mass calcd for $C_{13}H_{11}ClN_4O_4S$ (m/z) 377.0081 [M + Na]$^+$; found, 377.0070. mp 212 °C (dec). HPLC-UV (λ = 287 nm), purity 100%.

*7-[(2,4-Dichlorophenyl)sulfonyl]-1,3-dimethyl-3,7-dihydro-1H-purine-2,6-dione (**32**).* Following method B, theophylline (100 mg, 0.55 mmol), 2,4-dichlorobenzenesulfonyl chloride (163 mg, 0.67 mmol), and NaH (60% dispersion in mineral oil, 27 mg, 0.67 mmol) in THF (11 mL) yielded **32** as a white powder (160 mg, 74%) after purification by CC (gradient of EtOAc in hexane, 12/88 to 95/5). ^{1}H NMR (300 MHz, $CDCl_3$): δ 8.59 (d, J = 9.2 Hz, 1H, H6′), 8.43 (s, 1H, H8), 7.61−7.47 (m, 2H, H3′, H5′), 3.60 (s, 3H, N3CH_3), 3.30 (s, 3H, N1CH_3). ^{13}C NMR (75.4 MHz, $CDCl_3$): δ 152.9, 151.2, 150.6, 144.0, 142.9, 136.2, 133.9, 132.0, 131.7, 127.9, 105.7, 30.3, 28.6. HRMS (ESI$^+$) mass calcd for $C_{13}H_{10}Cl_2N_4O_4S$ (m/z) 410.9692 [M + Na]$^+$; found, 410.9687. mp 206−208 °C. Anal. Calcd for $C_{13}H_{10}Cl_2N_4O_4S$: C, 40.12; H, 2.59; N, 14.40; S, 8.24. Found: C, 40.19; H, 2.71; N, 14.22; S, 8.25.

*7-[(2-Chloro-4-fluorophenyl)sulfonyl]-1,3-dimethyl-3,7-dihydro-1H-purine-2,6-dione (**33**).* Following method B, theophylline (100 mg, 0.55 mmol), 2-chloro-4-fluorobenzenesulfonyl chloride (97 μL, 0.67 mmol), and NaH (60% dispersion in mineral oil, 27 mg, 0.67 mmol) in THF (11 mL) yielded **33** as a white powder (112 mg, 54%) after purification by CC (gradient of EtOAc in hexane, 12/88 to 100/0). ^{1}H NMR (300 MHz, $CDCl_3$): δ 8.69 (dd, J = 9.0, 5.7 Hz, 1H,

https://dx.doi.org/10.1021/acs.jmedchem.0c02145
J. Med. Chem. 2021, 64, 2272−2290

H6′), 8.43 (s, 1H, H8), 7.34−7.20 (m, 2H, H3′, H5′), 3.60 (s, 3H, N3CH$_3$), 3.29 (s, 3H, N1CH$_3$). ^{13}C NMR (75.4 MHz, CDCl$_3$): δ 166,4 (d, J = 263.9 Hz), 153.0, 151.3, 150.6, 144.0, 138.0 (d, J = 10.6 Hz), 135.2 (d, J = 11.3 Hz), 134.3, 129.8, 119.6 (d, J = 25.6 Hz), 115.1 (d, J = 21.9 Hz), 105.8, 30.3, 28.6. HRMS (ESI$^+$) mass calcd for $C_{13}H_{10}ClFN_4O_4S$ (m/z) 394.9987 [M + Na]$^+$; found, 394.9980. mp 220−222 °C. Anal. Calcd for $C_{13}H_{10}ClFN_4O_4S$: C, 41.89; H, 2.70; N, 15.03; S, 8.60. Found: C, 41.85; H, 2.82; N, 14.85; 8.72.

*7-([2-Chloro-4-(trifluoromethyl)phenyl]sulfonyl)-1,3-dimethyl-3,7-dihydro-1H-purine-2,6-dione (**34**).* Following method B, theophylline (100 mg, 0.55 mmol), 2-chloro-4-(trifluoromethyl)-benzenesulfonyl chloride (186 mg, 0.67 mmol), and NaH (60% dispersion in mineral oil, 27 mg, 0.67 mmol) in THF (11 mL) yielded **34** as a white powder (177 mg, 75%) after purification by CC (gradient of EtOAc in hexane, 15/85 to 100/0). ^{1}H NMR (300 MHz, CDCl$_3$): δ 8.80 (d, J = 8.4 Hz, 1H, H6′), 8.46 (s, 1H, H8), 7.84 (dd, J = 8.4, 1.7 Hz, 1H, H5′), 7.75 (d, J = 1.7 Hz, 1H, H3′), 3.60 (s, 3H, N3CH$_3$), 3.28 (s, 3H, N1CH$_3$). ^{13}C NMR (75.4 MHz, CDCl$_3$): δ 153.0, 151.2, 150.6, 144.0, 138.0 (q, J = 31.7 Hz), 136.92, 136.1, 133.9, 129.0 (q, J = 3.8 Hz), 124.4 (q, J = 3.8 Hz), 122.2 (d, J = 273.7 Hz), 105.8, 30.4, 28.6. HRMS (ESI$^+$) mass calcd for $C_{14}H_{10}ClF_3N_4O_4S$ (m/z) 444.9955 [M + Na]$^+$; found, 444.9954. mp 210 °C (dec). Anal. Calcd for $C_{14}H_{10}ClF_3N_4O_4S$: C, 39.77; H, 2.38; N, 13.25; S, 7.58. Found: C, 39.93; H, 2.55; N, 12.99; S, 7.76.

*7-[(2,4-Difluorophenyl)sulfonyl]-1,3-dimethyl-3,7-dihydro-1H-purine-2,6-dione (**35**).* Following method B, theophylline (100 mg, 0.55 mmol), 2,4-difluorobenzenesulfonyl chloride (141 mg, 0.67 mmol), and NaH (60% dispersion in mineral oil, 27 mg, 0.67 mmol) in THF (11 mL) yielded **35** as a white powder (142 mg, 72%) after purification by CC (gradient of EtOAc in hexane, 10/90 to 80/20). ^{1}H NMR (300 MHz, CDCl$_3$): δ 8.48 (ddd, J = 9.0, 8.1, 5.9 Hz, 1H, H6′), 8.37 (d, J = 1.2 Hz, 1H, H8), 7.16 (dddd, J = 8.9, 7.6, 2.4, 1.1 Hz, 1H, H5′), 6.93 (ddd, J = 10.4, 8.2, 2.4 Hz, 1H, H3′), 3.60 (s, 3H, N3CH$_3$), 3.31 (s, 3H, N1CH$_3$). ^{13}C NMR (75.4 MHz, CDCl$_3$): δ 167.8 (dd, J = 12.1, 262.4 Hz), 160.5 (dd, J = 12.8, 261.6 Hz), 153.0, 151.3, 150.6, 143.0, 135.8 (d, J = 11.31 Hz), 120.8 (dd, J = 3.8, 12.1 Hz), 112.7 (dd, J = 3.8, 22.6 Hz), 105.9 (dd, J = 24.9, 26.4 Hz), 105.8, 30.3, 28.6. HRMS (ESI$^+$) mass calcd for $C_{13}H_{10}F_2N_4O_4S$ (m/z) 379.0283 [M + Na]$^+$; found, 379.0269. Mp 194 °C (dec). Anal. Calcd for $C_{13}H_{10}F_2N_4O_4S$: C, 43.82; H, 2.83; N, 15.72; S, 9.00. Found: C, 43.83; H, 2.96; N, 15.63; S, 9.12.

*7-[(4-Fluoro-2-methylphenyl)sulfonyl]-1,3-dimethyl-3,7-dihydro-1H-purine-2,6-dione (**36**).* Following method B, theophylline (100 mg, 0.55 mmol), 4-fluoro-2-methylbenzenesulfonyl chloride (97 μL, 0.67 mmol), and NaH (60% dispersion in mineral oil, 27 mg, 0.67 mmol) in THF (11 mL) yielded **36** as a white powder (152 mg, 78%) after purification by CC (gradient of EtOAc in hexane, 10/90 to 80/20). ^{1}H NMR (300 MHz, CDCl$_3$): δ 8.57 (dd, J = 9.0, 5.5 Hz, 1H, H6′), 8.38 (s, 1H, H8), 7.17 (ddd, J = 9.5, 7.6, 2.6 Hz, 1H, H5′), 6.99 (dd, J = 9.0, 2.6, 1H, H3′), 3.59 (s, 3H, N3CH$_3$), 3.30 (s, 3H, N1CH$_3$), 2.51 (s, 3H, C2′CH$_3$). ^{13}C NMR (75.4 MHz, CDCl$_3$): δ 166.6 (d, J = 263.1 Hz), 153.0, 151.3, 150.6, 142.7, 142.2 (d, J = 9.8 Hz), 137.1 (d, J = 10.6 Hz), 130.3 (d, J = 3.0 Hz), 119.7 (d, J = 22.6 Hz), 114.1 (d, J = 21.9 Hz), 106.1, 30.3, 28.6, 20.4 (d, J = 1.1 Hz). HRMS (ESI$^+$) mass calcd for $C_{14}H_{13}FN_4O_4S$ (m/z) 375.0533 [M + Na]$^+$; found, 375.0535. mp 216−218 °C (dec). Anal. Calcd for $C_{14}H_{13}FN_4O_4S$: C, 47.72; H, 3.72; N, 15.90; S, 9.10. Found: C, 47.63; H, 3.83; N, 15.64; S, 9.18.

*7-[(2,5-Dichlorophenyl)sulfonyl]-1,3-dimethyl-3,7-dihydro-1H-purine-2,6-dione (**37**).* Following method B, theophylline (100 mg, 0.55 mmol), 2,5-dichlorobenzenesulfonyl chloride (163 mg, 0.67 mmol), and NaH (60% dispersion in mineral oil, 27 mg, 0.67 mmol) in THF (11 mL) yielded **37** as a white powder (157 mg, 73%) after purification by CC (gradient of EtOAc in hexane, 15/85 to 100/0). ^{1}H NMR (300 MHz, CDCl$_3$): δ 8.62 (d, J = 2.5 Hz, 1H, H6′), 8.43 (s, 1H, H8), 7.60 (dd, J = 8.6, 2.5 Hz, 1H, H4′), 7.42 (d, J = 8.6 Hz, 1H, H3′), 3.59 (s, 3H, N3CH$_3$), 3.30 (s, 3H, N1CH$_3$). ^{13}C NMR (75.4 MHz, CDCl$_3$): δ 152.8, 151.3, 150.5, 144.0, 136.4, 134.9, 134.8, 133.8, 132.8, 131.1, 105.8, 30.3, 28.6. HRMS (ESI$^+$) mass calcd for $C_{13}H_{10}Cl_2N_4O_4S$ (m/z) 410.9692 [M + Na]$^+$; found, 410.9686. mp 222 °C (dec). Anal. Calcd for $C_{13}H_{10}Cl_2N_4O_4S$: C, 40.12; H, 2.59; N, 14.40; S, 8.24. Found: C, 40.34; H, 2.78; N, 14.23; S, 8.52.

*7-[(4-Fluorophenyl)sulfonyl]-1,3-dimethyl-3,7-dihydro-1H-purine-2,6-dione (**38**).* Following method B, theophylline (100 mg, 0.55 mmol), 4-fluorobenzenesulfonyl chloride (130 mg, 0.67 mmol), and NaH (60% dispersion in mineral oil, 27 mg, 0.67 mmol) in THF (11 mL) yielded **38** as a white powder (152 mg, 81%) after purification by CC (gradient of EtOAc in hexane, 10/90 to 100/0). ^{1}H NMR (300 MHz, CDCl$_3$): δ 8.42−8.21 (m, 3H, H2′, H8), 7.36−7.20 (m, 2H, H3′), 3.57 (s, 3H, N3CH$_3$), 3.36 (s, 3H, N1CH$_3$). ^{13}C NMR (75.4 MHz, CDCl$_3$): δ 166.9 (d, J = 260.13), 153.1, 151.3, 150.8, 142.2, 133.0 (d, J = 10.6 Hz), 132.4 (d, J = 3.1 Hz), 117.1 (d, J = 22.6 Hz), 106.1, 30.3, 28.7. HRMS (ESI$^+$) mass calcd for $C_{13}H_{11}FN_4O_4S$ (m/z) 361.0377 [M + Na]$^+$ and 699.0862 [2M + Na]$^+$; found, 361.0366 and 699.0841. mp 223 °C (dec). Anal. Calcd for $C_{13}H_{11}FN_4O_4S$: C, 46.15; H, 3.28; N, 16.56; S, 9.48. Found: C, 46.05; H, 3.41; N, 16.45; S, 9.21.

Synthesis of 2-Chloro-1-(2-chlorobenzyl)-9-methyl-1,9-dihydro-6*H*-purin-6-one (40). Following the procedure described by Szarek et al.,[72] NaHCO$_3$ (35 mg, 0.42 mmol) was added to a solution of intermediate **39** (24 mg, 0.13 mmol) in DMF (1 mL). The reaction was stirred at rt for 30 min. 1-Chloro-2-(chloromethyl)-benzene (40 μL, 0.31 mmol) was added dropwise, and the mixture was heated up to 75 °C and stirred overnight. The solvent was evaporated under reduced pressure, and the residue was suspended in water (3 mL) and extracted with EtOAc (3 × 2 mL). The combined organic layer was washed with brine, dried over anhydrous Na$_2$SO$_4$, and filtered, and the solvent was evaporated under reduced pressure. Purification was performed by CC (gradient of EtOAc in hexane, 15/85 to 80/20), giving **40** as a brownish powder (10 mg, 32%). ^{1}H NMR (300 MHz, acetone-d_6): δ 8.44 (s, 1H, H8), 7.51 (dd, J = 7.8, 1.5 Hz, 1H, H3′), 7.35 (m, 2H, H4′, H5′), 7.08 (dd, J = 7.6, 1.9 Hz, 1H, H6′), 5.77 (s, 2H, CH$_2$), 4.07 (s, 3H, CH$_3$). ^{13}C NMR (75.4 MHz, acetone-d_6): δ 161.4, 153.8, 152.3, 143.8, 133.5, 132.8, 129.9, 129.8, 129.7, 127.6, 120.3, 54.4, 45.0. HRMS (ESI$^+$) mass calcd for $C_{13}H_{10}Cl_2N_4O$ (m/z) 309.0304 [M + H]$^+$; found, 309.0308. mp 146−149 °C. HPLC-UV (λ = 250 nm): purity 95%.

HEK293-hP2X7 Cell Culture. The human embryonic kidney cell line that stably expresses the human P2X7 isoform A (hP2X7-HEK293) was generously donated by Francesco di Virgilio's group. HEK293-hP2X7 cells were kept in 75 cm^2 flasks under DMEM-F12 culture medium enriched with 50 units/mL of penicillin and 50 μg/mL of streptomycin, 10% FBS bovine serum, and 0.2 mg/mL of geneticin (G-418 sulfate, Roche Diagnostics GmbH, Mannheim, Germany), which was used as a selection reagent. Cells were allowed to grow up to 95% confluence in an incubator with a constant atmosphere of 5% CO$_2$, saturated humidity, and at a temperature of 37 °C. For culture plating, they were dissociated from the flask using Trypsin−EDTA 0.05%, counted, and seeded in 96-well black, clear-bottomed plates (Conning Inc. Kennebunk ME, USA) at a different density depending on the experiment. Experiments were performed 24−48 h after plating.

YO-PRO-1 Uptake. hP2X7-HEK293 cells were seeded at a density of 400,000 cells/well. After 48 h, the culture medium was harvested and the cells were incubated with Mg^{2+}-free Krebs-HEPES buffer containing (in mM) 144 NaCl, 5.9 KCl, 11 glucose, 10 HEPES, and 0.2 CaCl$_2$ at pH 7.4. Test groups were incubated with the compounds for 20 min; then, the YOPRO-1 probe (2 μM) was applied, and subsequently, the cells were stimulated with BzATP (30 μM). Changes in the fluorescence (excitation at 485 nm and emission at 520 nm) were measured for 25 min using a fluorescence plate reader (Fluostar, BMG Labtech, Offenburg, Germany). Responses of each well were normalized with respect to the maximum (F_{max}) and the minimum (F_{min}) fluorescence values obtained by adding 0.5% Triton X-100 and then 2 M MnCl$_2$. Data were calculated with the formula $F = (F_x - F_0)/(F_{max} - F_{min})$, where F_x is the maximum fluorescence obtained and F_0 is the averaged fluorescence before Bz-ATP injection.

Fura-2 Calcium Measurements. hP2X7-HEK293 cells were seeded at a density of 50,000 cells/well and after 24−48 h were loaded with 8 μM Fura-2-AM (Invitrogen or Biotium, USA) for 1 h at

https://dx.doi.org/10.1021/acs.jmedchem.0c02145
J. Med. Chem. 2021, 64, 2272−2290

37 °C. After incubation, the loading medium was washed with Tyrode solution without Mg^{2+} (in mM): 137 NaCl, 10 HEPES, 2 $CaCl_2$, 4 KCl, and 10 glucose at pH 7.4, for 15−30 min. Test molecules were incubated during this period. Fura-2 calcium measurements were carried out with a fluorescence multi-well plate reader (Fluostar Optima, BMG, Germany). Cells were alternatively illuminated by 340 and 380 nm wavelength lights, and the emitted fluorescence was detected through a 520/10 nm filter for both excitation wavelengths. After a few cycles of basal fluorescence recording, the P2X7 agonist BzATP was injected to get a final concentration of 100 μM. Fluorescence was transformed to $[Ca^{2+}]_c$ with Grynkiewitz's equation.[73] Each experimental condition was performed in triplicate and averaged. Blockade is expressed as a percentage of the maximum $[Ca^{2+}]_c$ increase elicited by BzATP in control Tyrode-only wells.

Electrophysiological Measurements. cDNA of human His-P2X7 was synthesized (GeneArt String DNA fragment, Life Technologies/Thermo Fisher Scientific Inc.) and cloned together with the poly-A tail from the pNKS2 vector[74] into a modified pUC19 vector. Rat P2X7 cDNA was present in pSGem,[75] and rat P2X1 and P2X2 subunits were present in pNKS2.[74] Capped cRNAs were formed from linearized templates using the mMESSAGE mMACHINE Kit (Ambion, Austin, Texas, USA). Oocytes were kindly donated by Prof. Luis Pardo, MPI for Experimental Medicine, Göttingen or from EcoCyte Bioscience, Dortmund, Germany), injected with 50 nL of cRNA (0.5 mg/mL for rP2X1, rP2X4 and hP2X7; 0.1 mg/mL for rP2X2; 25 μg/mL for rP2X7), and incubated for 1−2 days at 16−18 °C before recordings were performed as described[76] in a low divalent-cation solution (90 mM NaCl, 1 mM KCl, 0.5 mM $CaCl_2$, 5 mM HEPES). Current responses to ATP (300 μM for hP2X7, 30 μM for rP2X4 and rP2X7, and 10 μM for rP2X2 and rP2X1) were measured by TEVC at −70 mV using a Turbo Tec 05X Amplifier (NPI Electronic, Tamm, Germany) and Cell Works software. A rapid exchange of solution, about 300 ms, was reached with a 50 μL oocyte chamber with a funnel shape, combined with a fast solution flow (150 μL/s), fed through a manifold built immediately above the oocyte. Compounds were directly diluted in the recording chamber and incubated for 3 min without perfusion. ATP pulses were applied for 2 s (3 s for rP2X7 subtype) followed by 58 s of perfusion at 4-min intervals. Data were shown as means ± S.E.M. from at least three oocytes from two different frogs.

Isolation of MPMs. Elicited MPMs were obtained from twelve (n = 12) 6−8 week-old C57BL/6 male mice. Twenty-four hours before macrophages extraction, mice were injected intraperitoneally with 1 mL of 3.8% Brewer's thioglycolate medium in order to attract circulating macrophages to the peritoneal cavity. The day after, the mice were euthanized by cervical dislocation and the abdominal skin was retracted to expose the peritoneal wall. The highest efforts were made to mitigate animal suffering according to the EU Council Directive guidelines. All experiments with animals were carried out in accordance with the ARRIVE guidelines, the International Council for Laboratory Animal Science and the European Union 2010/63/EU Guidelines. The experimental protocol was approved by the Institutional Ethical Committee for Animal Research at the Universidad Autónoma de Madrid (UAM). Ten milliliters of cold sterile PBS were injected in the peritoneal cavity with a 20-G needle, and the peritoneal content was collected by aspirating the fluid with the same syringe and needle. The peritoneal exudate cells were centrifuged at 4 °C for 10 min at 1000 rpm, and the cell pellet was resuspended in 1 mL of cold DMEM high glucose (Gibco) supplemented with 10% FBS (Gibco), 100 U/mL penicillin/streptomycin (Lonza). Cells were counted with a Neubauer chamber, and the cell concentration was adjusted to $1-3 \times 10^6$ cells/mL. Macrophages were seeded in 24-well plates at a density of 3×10^5 cells/well and primed with 1 μg/mL LPS (*Escherichia coli* 026:B6 serotype; Sigma-Aldrich) in DMEM high glucose +10% SBF for 4 h. The LPS-containing medium was removed and fresh DMEM without FBS containing the different compounds was added for 15 min. ATP 5 mM (Sigma-Aldrich) was then added for 30 min. Cell supernatants were collected and frozen at −20 °C for IL-1β detection.

IL-1β detection. IL-1β (pg/mL) was detected in the collected cell supernatants using a specific ELISA kit. Supernatant samples were obtained from the treated MPMs and subjected to the ELISA analysis according to the supplier recommendations (R&D systems).

Parallel Artificial Membrane Permeability Assay. The lipophilic membrane was prepared by dissolving porcine brain polar lipid extract (Avanti, Merck) in dodecane (Sigma-Aldrich) at a concentration of 20 mg/mL and injecting 4 μL of it on the membrane of each well of a 96-well Multiscreen Filter Plate (Reference: MAIPNTR10, Millipore, Merck). Compound solutions were prepared at 100 μM in PBS at pH 7.4 (Sigma-Aldrich, Merck). The blank solution contained 1% of DMSO. Each well was then filled with 180 μL of compounds or blank solution, whereas the corresponding wells of the acceptor Multiscreen 96-well tray (MAMCS9610, Millipore, Merck) were filled with an equal amount of PBS at pH 7.4. The filter plate was inserted in the acceptor tray and incubated at rt for 4 h. A volume of 150 μL of acceptor plate solutions was transferred to a UV-transparent 96-well plate (MSCPNUV40, Millipore, Merck) together with compound solutions at initial and equilibrium concentrations (100 μM and 50 μM, respectively). Compound absorption spectra were recorded by a SPECTROstar Nano Microplate Reader (BMG Labtech, Orterberg, Germany) and corrected by blank absorption spectra. Concentrations and permeability values were calculated with the following equations

$$P(10^{-6}\cdot\mathrm{cm}\cdot\mathrm{sec}^{-1}) = K\cdot -\ln(1 - C_{ac}/C_{eq})$$

$$K = \frac{V}{2 \cdot a \cdot t} \qquad C_{ac} = A_{ac}\cdot C_0/A_0$$

$$C_{eq} = A_{eq}\cdot C_0/A_0$$

where V is the solution volume (180 μL); a is the membrane area in cm^2; t is the time of incubation in seconds; C_0 is the starting concentration of compound solutions; A_0 is the measured absorbance of compound solutions at starting concentration; A_{eq} is the measured absorbance of the solution with concentration at equilibrium point, that is, when the compound completely permeates the membrane; and A_{ac} is the measured absorbance of solutions in the acceptor plate. For each compound, the wavelength at maximum absorbance was considered for calculations (240 nm for JNJ-47965567; 264 nm for **6**, **16**, **23**, **29**, **30**, and **40**; 274 nm for theophylline, **17**, and **24**; 284 nm for verapamil and **31**; 365 nm for piroxicam). All data are presented as mean ± S.E.M. of triplicates of three individual experiments performed in three different days.

Pgp ATP-ase Activity Measurements. Human P-glycoprotein ATPase activity was measured using the luminescence-based Pgp-glo Assay System (Promega, Madison, WI, USA). The assay was performed according to manufacturer's protocol (freely available at Promega webpage). Compounds were tested at 10 μM, and MgATP was incubated for 1.5 h. Data were acquired using a microplate luminometer (Orion II, Berthold Technologies GmbH& Co. KG, Germany) and processed according to the manufacturer's protocol. Briefly, basal relative luminescence unit (R.L.U) variation was calculated as the R.L.U. difference of Na_3VO_4-treated wells and non-treated wells R.L.U. Compounds R.L.U. variation was calculated as the R.L.U. difference of Na_3VO_4-treated wells and compound-treated wells.

Data Analysis. The statistically significant differences were analyzed by the one sample t-test or the one-way analysis of variance (ANOVA), followed by the Dunnett post hoc test, using Prism 5.0 (Graph Pad) under a Mac OS X-operated computer. Groups of data were considered statistically different when $p < 0.05$.

Molecular Docking. The ligand was docked with the consent of Dr. Ralf Schmid in the homology model of the hP2X7 published by Dayel et al.[11] Molecules' 3D conformations were generated using Open Babel.[77] The ligand was docked in two previously described allosteric binding pockets of hP2X7[9−11] and in the orthosteric binding pocket using a squared grid with a side of 22−26 Å. Docking was performed using AutodockTools and Autodock Vina[78] and represented using UCSF Chimera.[79]

https://dx.doi.org/10.1021/acs.jmedchem.0c02145
J. Med. Chem. 2021, 64, 2272−2290

■ ASSOCIATED CONTENT

Supporting Information

The Supporting Information is available free of charge at https://pubs.acs.org/doi/10.1021/acs.jmedchem.0c02145.

Scheme for the synthesis of **14**, summary of pharmacological data of the tested compounds, NMR spectra, current inhibition in rat P2X7 by **6**, HPLC, and X-ray (PDF)

Molecular formula strings (CSV)

PDB coordinates for the computational model used, modified from the protein model by Dayel et al.[11] with permission (crystal templates PDB IDs 5U1U,5U1V, 5U1W, 5U1X, 5U1Y) (TXT)

Compound **6** pose at the P2X7 binding site (MP4)

■ AUTHOR INFORMATION

Corresponding Authors

Antonio G. García − *Instituto-Fundación Teófilo Hernando and Departamento de Farmacología, Facultad de Medicina, Universidad Autónoma de Madrid, 28029 Madrid, Spain; Instituto de Investigación Sanitaria, Hospital Universitario de La Princesa, 28006 Madrid, Spain*; Phone: (+34) 914975397; Email: agg@uam.es; Fax: (+34)-914973453

Cristóbal de los Ríos − *Instituto-Fundación Teófilo Hernando and Departamento de Farmacología, Facultad de Medicina, Universidad Autónoma de Madrid, 28029 Madrid, Spain; Instituto de Investigación Sanitaria, Hospital Universitario de La Princesa, 28006 Madrid, Spain;* orcid.org/0000-0002-6456-7589; Phone: (+34)-914972765; Email: cristobal.delosrios@inv.uam.es

Authors

Francesco Calzaferri − *Instituto-Fundación Teófilo Hernando and Departamento de Farmacología, Facultad de Medicina, Universidad Autónoma de Madrid, 28029 Madrid, Spain;* orcid.org/0000-0002-4781-2925

Paloma Narros-Fernández − *Instituto-Fundación Teófilo Hernando and Departamento de Farmacología, Facultad de Medicina, Universidad Autónoma de Madrid, 28029 Madrid, Spain; Instituto de Investigación Sanitaria, Hospital Universitario de La Princesa, 28006 Madrid, Spain*

Ricardo de Pascual − *Instituto-Fundación Teófilo Hernando and Departamento de Farmacología, Facultad de Medicina, Universidad Autónoma de Madrid, 28029 Madrid, Spain*

Antonio M.G. de Diego − *Instituto-Fundación Teófilo Hernando and Departamento de Farmacología, Facultad de Medicina, Universidad Autónoma de Madrid, 28029 Madrid, Spain*

Annette Nicke − *Walther Straub Institute of Pharmacology and Toxicology, Faculty of Medicine, Ludwig-Maximilians-Universität München, 80336 Munich, Germany*

Javier Egea − *Instituto-Fundación Teófilo Hernando and Departamento de Farmacología, Facultad de Medicina, Universidad Autónoma de Madrid, 28029 Madrid, Spain; Instituto de Investigación Sanitaria, Hospital Universitario de La Princesa, 28006 Madrid, Spain;* orcid.org/0000-0003-4704-3019

Complete contact information is available at: https://pubs.acs.org/10.1021/acs.jmedchem.0c02145

Notes

The authors declare no competing financial interest.

■ ACKNOWLEDGMENTS

This work has been supported by the following grants: EU Horizon 2020 Research and Innovation Program under Marie Skłodowska-Curie, Grant Agreement N. 766124 to AGG and AN, and Ministerio de Economía y Competitividad, Spain, Grant Number SAF2016-78892R to AGG; Deutsche Forschungsgemeinschaft (DFG, German Research Foundation) Project-ID: 335447717, SFB 1328 (TP15) to A.N.; Instituto de Salud Carlos III, Ministerio de Economía y Competitividad, Spain, Grant Numbers PI16/01041 and PI19/01724 (Co-funded by FEDER) to CdlR; Instituto de Salud Carlos III, Ministerio de Economía y Competitividad, Spain, Grant Numbers PI16/00735 and PI19/00082 (Co-funded by FEDER) to J.E. We thank Fundación Teófilo Hernando for continuous support. We thank Prof. Francesco de Virgilio and his research group for the generous donation of hP2X7-HEK293 cells. We thank Prof. Luis Pardo for the generous donation of *X. laevis* oocytes. We thank Dr. Ralf Schmid for permission to use the homology model of hP2X7. We thank Dr. Eva M. Garcia-Frutos (ICMM, CSIC, Spain) for X-ray diffraction crystal preparation. We thank Dr. Juan Felipe Franco-Gonzalez (CIB, CSIC, Spain) for assistance with computational docking analyses.

■ ABBREVIATIONS

Aβ, amyloid β peptide; AD, Alzheimer's disease; ALS, amyothrophic lateral sclerosis; BBB, blood−brain barrier; BBG, brilliant blue G; CC, column chromatography; CNS, central nervous system; DMEM, Dulbecco-modified Eagle's medium; FBS, fetal bovine serum; IL-1β, interleukin 1β; MPMs, mouse peritoneal macrophages; NDDs, neurodegenerative diseases; PAMPA, parallel artificial membrane permeability assay; PD, Parkinson's disease; P2X, type 2 ionotropic purinergic receptor

■ REFERENCES

(1) DiLuca, M.; Olesen, J. The Cost of Brain Diseases: a Burden or a Challenge? *Neuron* **2014**, *82*, 1205−1208.

(2) Gustavsson, A.; Svensson, M.; Jacobi, F.; Allgulander, C.; Alonso, J.; Beghi, E.; Dodel, R.; Ekman, M.; Faravelli, C.; Fratiglioni, L.; Gannon, B.; Jones, D. H.; Jennum, P.; Jordanova, A.; Jönsson, L.; Karampampa, K.; Knapp, M.; Kobelt, G.; Kurth, T.; Lieb, R.; Linde, M.; Ljungcrantz, C.; Maercker, A.; Melin, B.; Moscarelli, M.; Musayev, A.; Norwood, F.; Preisig, M.; Pugliatti, M.; Rehm, J.; Salvador-Carulla, L.; Schlehofer, B.; Simon, R.; Steinhausen, H.-C.; Stovner, L. J.; Vallat, J.-M.; den Bergh, P. V.; van Os, J.; Vos, P.; Xu, W.; Wittchen, H.-U.; Jönsson, B.; Olesen, J.; Group, C. D. Cost of Disorders of the Brain in Europe 2010. *Eur. Neuropsychopharmacol.* **2011**, *21*, 718−779.

(3) Virgilio, F. P2X Receptors and Inflammation. *Curr. Med. Chem.* **2015**, *22*, 866−877.

(4) Calzaferri, F.; Ruiz-Ruiz, C.; Diego, A. M. G.; Pascual, R.; Méndez-López, I.; Cano-Abad, M. F.; Maneu, V.; Ríos, C.; Gandía, L.; García, A. G. The Purinergic P2X7 Receptor as a Potential Drug Target to Combat Neuroinflammation in Neurodegenerative Diseases. *Med. Res. Rev.* **2020**, *40*, 2427−2465.

(5) Surprenant, A.; Rassendren, F.; Kawashima, E.; North, R. A.; Buell, G. The Cytolytic P2Z Receptor for Extracellular ATP Identified as a P2X Receptor (P2X7). *Science* **1996**, *272*, 735−738.

(6) Denlinger, L. C.; Fisette, P. L.; Sommer, J. A.; Watters, J. J.; Prabhu, U.; Dubyak, G. R.; Proctor, R. A.; Bertics, P. J. Cutting Edge: the Nucleotide Receptor P2X7 Contains Multiple Protein- and Lipid-Interaction Motifs Including a Potential Binding Site for Bacterial Lipopolysaccharide. *J. Immunol.* **2001**, *167*, 1871−1876.

(7) Ferrari, D.; Pizzirani, C.; Adinolfi, E.; Lemoli, R. M.; Curti, A.; Idzko, M.; Panther, E.; Di Virgilio, F. The P2X7 Receptor: a Key Player in IL-1 Processing and Release. *J. Immunol.* **2006**, *176*, 3877−3883.
(8) Piccini, A.; Carta, S.; Tassi, S.; Lasiglie, D.; Fossati, G.; Rubartelli, A. ATP is Released by Monocytes Stimulated with Pathogen-Sensing Receptor Ligands and Induces IL-1beta and IL-18 Secretion in an Autocrine Way. *Proc. Natl. Acad. Sci. U.S.A.* **2008**, *105*, 8067−8072.
(9) Karasawa, A.; Kawate, T. Structural Basis for Subtype-Specific Inhibition of the P2X7 Receptor. *eLife* **2016**, *5*, No. e22153.
(10) Bidula, S. M.; Cromer, B. A.; Walpole, S.; Angulo, J.; Stokes, L. Mapping a Novel Positive Allosteric Modulator Binding Site in the Central Vestibule Region of Human P2X7. *Sci. Rep.* **2019**, *9*, 3231.
(11) Dayel, A. B.; Evans, R. J.; Schmid, R. Mapping the Site of Action of Human P2X7 Receptor Antagonists AZ11645373, Brilliant Blue G, KN-62, Calmidazolium, and ZINC58368839 to the Intersubunit Allosteric Pocket. *Mol. Pharmacol.* **2019**, *96*, 355−363.
(12) Caseley, E. A.; Muench, S. P.; Baldwin, S. A.; Simmons, K.; Fishwick, C. W.; Jiang, L.-H. Docking of Competitive Inhibitors to the P2X7 Receptor Family Reveals Key Differences Responsible for Changes in Response Between Rat and Human. *Bioorg. Med. Chem. Lett.* **2015**, *25*, 3164−3167.
(13) Parvathenani, L. K.; Tertyshnikova, S.; Greco, C. R.; Roberts, S. B.; Robertson, B.; Posmantur, R. P2X7 Mediates Superoxide Production in Primary Microglia and is Up-Regulated in a Transgenic Mouse Model of Alzheimer's Disease. *J. Biol. Chem.* **2003**, *278*, 13309−13317.
(14) Martinez-Frailes, C.; Di Lauro, C.; Bianchi, C.; de Diego-Garcia, L.; Sebastian-Serrano, A.; Bosca, L.; Diaz-Hernandez, M. Amyloid Peptide Induced Neuroinflammation Increases the P2X7 Receptor Expression in Microglial Cells, Impacting on Its Functionality. *Front. Cell. Neurosci.* **2019**, *13*, 143.
(15) Diaz-Hernandez, J. I.; Gomez-Villafuertes, R.; León-Otegui, M.; Hontecillas-Prieto, L.; Del Puerto, A.; Trejo, J. L.; Lucas, J. J.; Garrido, J. J.; Gualix, J.; Miras-Portugal, M. T.; Diaz-Hernandez, M. In vivo P2X7 inhibition reduces amyloid plaques in Alzheimer's disease through GSK3β and secretases. *Neurobiol. Aging* **2012**, *33*, 1816−1828.
(16) Durrenberger, P. F.; Grünblatt, E.; Fernando, F. S.; Monoranu, C. M.; Evans, J.; Riederer, P.; Reynolds, R.; Dexter, D. T. Inflammatory Pathways in Parkinson's Disease; A BNE Microarray Study. *Parkinsons Dis.* **2012**, *2012*, 214714.
(17) Jun, D.-J.; Kim, J.; Jung, S.-Y.; Song, R.; Noh, J.-H.; Park, Y.-S.; Ryu, S.-H.; Kim, J.-H.; Kong, Y.-Y.; Chung, J.-M.; Kim, K.-T. Extracellular ATP Mediates Necrotic Cell Swelling in SN4741 Dopaminergic Neurons Through P2X7 Receptors. *J. Biol. Chem.* **2007**, *282*, 37350−37358.
(18) Carmo, M. R. S.; Menezes, A. P. F.; Nunes, A. C. L.; Pliássova, A.; Rolo, A. P.; Palmeira, C. M.; Cunha, R. A.; Canas, P. M.; Andrade, G. M. The P2X7 Receptor Antagonist Brilliant Blue G Attenuates Contralateral Rotations in a Rat Model of Parkinsonism Through a Combined Control of Synaptotoxicity, Neurotoxicity and Gliosis. *Neuropharmacol* **2014**, *81*, 142−152.
(19) Ferrazoli, E. G.; de Souza, H. D. N.; Nascimento, I. C.; Oliveira-Giacomelli, Á.; Schwindt, T. T.; Britto, L. R.; Ulrich, H. Brilliant Blue G, But Not Fenofibrate, Treatment Reverts Hemiparkinsonian Behavior and Restores Dopamine Levels in an Animal Model of Parkinson's Disease. *Cell Transplant.* **2017**, *26*, 669−677.
(20) Ruiz-Ruiz, C.; Calzaferri, F.; Garcia, A. G. P2X7 Receptor Antagonism as a Potential Therapy in Amyotrophic Lateral Sclerosis. *Front. Mol. Neurosci.* **2020**, *13*, 93.
(21) Yiangou, Y.; Facer, P.; Durrenberger, P.; Chessell, I. P.; Naylor, A.; Bountra, C.; Banati, R. R.; Anand, P. COX-2, CB2 and P2X7-Immunoreactivities are Increased in Activated Microglial Cells/Macrophages of Multiple Sclerosis and Amyotrophic Lateral Sclerosis Spinal Cord. *BMC Neurol.* **2006**, *6*, 12.
(22) Cervetto, C.; Frattaroli, D.; Maura, G.; Marcoli, M. Motor Neuron Dysfunction in a Mouse Model of ALS: Gender-Dependent Effect of P2X7 Antagonism. *Toxicol* **2013**, *311*, 69−77.
(23) Ly, D.; Dongol, A.; Cuthbertson, P.; Guy, T. V.; Geraghty, N. J.; Sophocleous, R. A.; Sin, L.; Turner, B. J.; Watson, D.; Yerbury, J. J.; Sluyter, R. The P2X7 Receptor Antagonist JNJ-47965567 Administered Thrice Weekly from Disease Onset Does not Alter Progression of Amyotrophic Lateral Sclerosis in SOD1(G93A) Mice. *Purinergic Signal.* **2020**, *16*, 109−122.
(24) Narcisse, L.; Scemes, E.; Zhao, Y.; Lee, S. C.; Brosnan, C. F. The Cytokine IL-1beta Transiently Enhances P2X7 Receptor Expression and Function in Human Astrocytes. *Glia* **2005**, *49*, 245−258.
(25) Guile, S. D.; Alcaraz, L.; Birkinshaw, T. N.; Bowers, K. C.; Ebden, M. R.; Furber, M.; Stocks, M. J. Antagonists of the P2X(7) Receptor. From Lead Identification to Drug Development. *J. Med. Chem.* **2009**, *52*, 3123−3141.
(26) Murgia, M.; Hanau, S.; Pizzo, P.; Rippa, M.; Di Virgilio, F. Oxidized ATP. An Irreversible Inhibitor of the Macrophage Purinergic P2Z Receptor. *J. Biol. Chem.* **1993**, *268*, 8199−8203.
(27) Peng, W.; Cotrina, M. L.; Han, X.; Yu, H.; Bekar, L.; Blum, L.; Takano, T.; Tian, G.-F.; Goldman, S. A.; Nedergaard, M. Systemic Administration of an Antagonist of the ATP-Sensitive Receptor P2X7 Improves Recovery after Spinal Cord Injury. *Proc. Natl. Acad. Sci. U.S.A.* **2009**, *106*, 12489−12493.
(28) Lambrecht, G.; Friebe, T.; Grimm, U.; Windscheif, U.; Bungardt, E.; Hildebrandt, C.; Bäumert, H. G.; Spatz-Kümbel, G.; Mutschler, E. PPADS, a Novel Functionally Selective Antagonist of P2 Purinoceptor-Mediated Responses. *Eur. J. Pharmacol.* **1992**, *217*, 217−219.
(29) Gargett, C. E.; Wiley, J. S. The Isoquinoline Derivative KN-62 a Potent Antagonist of the P2Z-Receptor of Human Lymphocytes. *Br. J. Pharmacol.* **1997**, *120*, 1483−1490.
(30) Park, J.-H.; Lee, G.-E.; Lee, S.-D.; Ko, H.; Kim, Y.-C. Structure-Activity Relationship Studies of Pyrimidine-2,4-dione Derivatives as Potent P2X7 Receptor Antagonists. *Eur. J. Med. Chem.* **2015**, *106*, 180−193.
(31) Lee, G. E.; Lee, H.-S.; Lee, S. D.; Kim, J.-H.; Kim, W.-K.; Kim, Y.-C. Synthesis and Structure-Activity Relationships of Novel, Substituted 5,6-dihydrodibenzo[a,g]quinolizinium P2X7 Antagonists. *Bioorg. Med. Chem. Lett.* **2009**, *19*, 954−958.
(32) O'Brien-Brown, J.; Jackson, A.; Reekie, T. A.; Barron, M. L.; Werry, E. L.; Schiavini, P.; McDonnell, M.; Munoz, L.; Wilkinson, S.; Noll, B.; Wang, S.; Kassiou, M. Discovery and Pharmacological Evaluation of a Novel Series of Adamantyl Cyanoguanidines as P2X7 Receptor Antagonists. *Eur. J. Med. Chem.* **2017**, *130*, 433−439.
(33) Merriman, G. H.; Ma, L.; Shum, P.; McGarry, D.; Volz, F.; Sabol, J. S.; Gross, A.; Zhao, Z.; Rampe, D.; Wang, L.; Wirtz-Brugger, F.; Harris, B. A.; Macdonald, D. Synthesis and SAR of Novel 4,5-Diarylimidazolines as Potent P2X7 Receptor Antagonists. *Bioorg. Med. Chem. Lett.* **2005**, *15*, 435−438.
(34) Lee, J.-Y.; Yu, J.; Cho, W. J.; Ko, H.; Kim, Y.-C. Synthesis and Structure-Activity Relationships of Pyrazolodiazepine Derivatives as Human P2X7 Receptor Antagonists. *Bioorg. Med. Chem. Lett.* **2009**, *19*, 6053−6058.
(35) Park, J.-H.; Williams, D. R.; Lee, J.-H.; Lee, S.-D.; Lee, J.-H.; Ko, H.; Lee, G.-E.; Kim, S.; Lee, J.-M.; Abdelrahman, A.; Müller, C. E.; Jung, D.-W.; Kim, Y.-C. Potent Suppressive Effects of 1-Piperidinylimidazole Based Novel P2X7 Receptor Antagonists on Cancer Cell Migration and Invasion. *J. Med. Chem.* **2016**, *59*, 7410−7430.
(36) Kwak, S.-H.; Shin, S.; Lee, J.-H.; Shim, J.-K.; Kim, M.; Lee, S.-D.; Lee, A.; Bae, J.; Park, J.-H.; Abdelrahman, A.; Müller, C. E.; Cho, S. K.; Kang, S.-G.; Bae, M. A.; Yang, J. Y.; Ko, H.; Goddard, W. A., 3rd; Kim, Y.-C. Synthesis and Structure-Activity Relationships of Quinolinone and Quinoline-Based P2X7 Receptor Antagonists and Their anti-Sphere Formation Activities in Glioblastoma Cells. *Eur. J. Med. Chem.* **2018**, *151*, 462−481.

https://dx.doi.org/10.1021/acs.jmedchem.0c02145
J. Med. Chem. 2021, 64, 2272−2290

(37) Xiao, Y.; Karra, S.; Goutopoulos, A.; Morse, N. T.; Zhang, S.; Dhanabal, M.; Tian, H.; Seenisamy, J.; Jayadevan, J.; Caldwell, R.; Potnick, J.; Bleich, M.; Chekler, E.; Sherer, B.; Sriraman, V. Synthesis and SAR Development of Quinoline Analogs as Novel P2X7 Receptor Antagonists. *Bioorg. Med. Chem. Lett.* **2019**, *29*, 1660−1664.
(38) Faria, R. X.; de Jesus Hiller, N.; Salles, J. P.; Resende, J. A. L. C.; Diogo, R. T.; von Ranke, N. L.; Bello, M. L.; Rodrigues, C. R.; Castro, H. C.; de Luna Martins, D. Arylboronic Acids Inhibit P2X7 Receptor Function and the Acute Inflammatory Response. *J. Bioenerg. Biomembr.* **2019**, *51*, 277−290.
(39) Gonzaga, D. T. G.; Oliveira, F. H.; von Ranke, N. L.; Pinho, G. Q.; Salles, J. P.; Bello, M. L.; Rodrigues, C. R.; Castro, H. C.; de Souza, H.; Reis, C. R. C.; Leme, R. P. P.; Mafra, J. C. M.; Pinheiro, L. C. S.; Hoelz, L. V. B.; Boechat, N.; Faria, R. X. Synthesis, Biological Evaluation, and Molecular Modeling Studies of New Thiadiazole Derivatives as Potent P2X7 Receptor Inhibitors. *Front. Chem.* **2019**, *7*, 261.
(40) Perez-Medrano, A.; Donnelly-Roberts, D. L.; Florjancic, A. S.; Nelson, D. W.; Li, T.; Namovic, M. T.; Peddi, S.; Faltynek, C. R.; Jarvis, M. F.; Carroll, W. A. Synthesis and in Vitro Activity of N-benzyl-1-(2,3-dichlorophenyl)-1H-tetrazol-5-amine P2X(7) Antagonists. *Bioorg. Med. Chem. Lett.* **2011**, *21*, 3297−3300.
(41) Savall, B. M.; Wu, D.; De Angelis, M.; Carruthers, N. I.; Ao, H.; Wang, Q.; Lord, B.; Bhattacharya, A.; Letavic, M. A. Synthesis, SAR, and Pharmacological Characterization of Brain Penetrant P2X7 Receptor Antagonists. *ACS Med. Chem. Lett.* **2015**, *6*, 671−676.
(42) Abdi, M. H.; Beswick, P. J.; Billinton, A.; Chambers, L. J.; Charlton, A.; Collins, S. D.; Collis, K. L.; Dean, D. K.; Fonfria, E.; Gleave, R. J.; Lejeune, C. L.; Livermore, D. G.; Medhurst, S. J.; Michel, A. D.; Moses, A. P.; Page, L.; Patel, S.; Roman, S. A.; Senger, S.; Slingsby, B.; Steadman, J. G. A.; Stevens, A. J.; Walter, D. S. Discovery and Structure-Activity Relationships of a Series of Pyroglutamic Acid Amide Antagonists of the P2X7 Receptor. *Bioorg. Med. Chem. Lett.* **2010**, *20*, 5080−5084.
(43) Honore, P.; Donnelly-Roberts, D.; Namovic, M. T.; Hsieh, G.; Zhu, C. Z.; Mikusa, J. P.; Hernandez, G.; Zhong, C.; Gauvin, D. M.; Chandran, P.; Harris, R.; Medrano, A. P.; Carroll, W.; Marsh, K.; Sullivan, J. P.; Faltynek, C. R.; Jarvis, M. F. A-740003 [N-(1-{[(cyanoimino)(5-quinolinylamino) methyl]amino}-2,2-dimethylpropyl)-2-(3,4-dimethoxyphenyl)acetamide], a Novel and Selective P2X7 Receptor Antagonist, Dose-Dependently Reduces Neuropathic Pain in the Rat. *J. Pharmacol. Exp. Ther.* **2006**, *319*, 1376−1385.
(44) Donnelly-Roberts, D. L.; Namovic, M. T.; Surber, B.; Vaidyanathan, S. X.; Perez-Medrano, A.; Wang, Y.; Carroll, W. A.; Jarvis, M. F. [3H]A-804598 ([3H]2-cyano-1-[(1S)-1-phenylethyl]-3-quinolin-5-ylguanidine) is a Novel, potent, and selective antagonist radioligand for P2X7 receptors. *Neuropharmacol* **2009**, *56*, 223−229.
(45) Chrovian, C. C.; Soyode-Johnson, A.; Peterson, A. A.; Gelin, C. F.; Deng, X.; Dvorak, C. A.; Carruthers, N. I.; Lord, B.; Fraser, I.; Aluisio, L.; Coe, K. J.; Scott, B.; Koudriakova, T.; Schoetens, F.; Sepassi, K.; Gallacher, D. J.; Bhattacharya, A.; Letavic, M. A. A Dipolar Cycloaddition Reaction To Access 6-Methyl-4,5,6,7-tetrahydro-1H-[1,2,3]triazolo[4,5-c]pyridines Enables the Discovery Synthesis and Preclinical Profiling of a P2X7 Antagonist Clinical Candidate. *J. Med. Chem.* **2018**, *61*, 207−223.
(46) Letavic, M. A.; Savall, B. M.; Allison, B. D.; Aluisio, L.; Andres, J. I.; De Angelis, M.; Ao, H.; Beauchamp, D. A.; Bonaventure, P.; Bryant, S.; Carruthers, N. I.; Ceusters, M.; Coe, K. J.; Dvorak, C. A.; Fraser, I. C.; Gelin, C. F.; Koudriakova, T.; Liang, J.; Lord, B.; Lovenberg, T. W.; Otieno, M. A.; Schoetens, F.; Swanson, D. M.; Wang, Q.; Wickenden, A. D.; Bhattacharya, A. 4-Methyl-6,7-dihydro-4H-triazolo[4,5-c]pyridine-Based P2X7 Receptor Antagonists: Optimization of Pharmacokinetic Properties Leading to the Identification of a Clinical Candidate. *J. Med. Chem.* **2017**, *60*, 4559−4572.
(47) US National Library of Medicine. https://clinicaltrials.gov/, (accessed Jan 15, 2021).
(48) Recourt, K.; van der Aart, J.; Jacobs, G.; de Kam, M.; Drevets, W.; van Nueten, L.; Kanhai, K.; Siebenga, P.; Zuiker, R.; Ravenstijn, P.; Timmers, M.; van Gerven, J.; de Boer, P. Characterisation of the Pharmacodynamic Effects of the P2X7 Receptor Antagonist JNJ-54175446 Using an Oral Dexamphetamine Challenge Model in Healthy Males in a Randomised, Double-Blind, Placebo-Controlled, Multiple Ascending Dose Trial. *J. Psychopharmacol.* **2020**, *34*, 1030−1042.
(49) Keystone, E. C.; Wang, M. M.; Layton, M.; Hollis, S.; McInnes, I. B.; Team, D. C. S. Clinical Evaluation of the Efficacy of the P2X7 Purinergic Receptor Antagonist AZD9056 on the Signs and Symptoms of Rheumatoid Arthritis in Patients with Active Disease Despite Treatment with Methotrexate or Sulphasalazine. *Ann. Rheum. Dis.* **2012**, *71*, 1630−1635.
(50) Eser, A.; Colombel, J. F.; Rutgeerts, P.; Vermeire, S.; Vogelsang, H.; Braddock, M.; Persson, T.; Reinisch, W. Safety and Efficacy of an Oral Inhibitor of the Purinergic Receptor P2X7 in Adult Patients with Moderately to Severely Active Crohn's Disease: A Randomized Placebo-controlled, Double-blind, Phase IIa Study. *Inflamm. Bowel Dis.* **2015**, *21*, 2247−2253.
(51) Jacobson, K.; Costanzi, S.; Ohno, M.; Joshi, B.; Besada, P.; Xu, B.; Tchilibon, S. Molecular Recognition at Purine and Pyrimidine Nucleotide (P2) Receptors. *Curr. Top. Med. Chem.* **2004**, *4*, 805−819.
(52) Soltani Rad, M. N.; Behrouz, S.; Asrari, Z.; Khalafi-Nezhad, A. A Simple and Regioselective One-Pot Procedure for the Direct N-Acylation of Some Purine and Pyrimidine Nucleobases via Carboxylic Acids Using Cyanuric Chloride. *Monatsh. Chem.* **2014**, *145*, 1933−1940.
(53) Tumma, H.; Nagaraju, N.; Reddy, K. V. N-Alkylation of 2,6-Dichloropurine Hydrochloride with a Variety of Alcohols over Alumina Catalyst. *Synth. Commun.* **2010**, *40*, 1856−1866.
(54) Rat, P.; Olivier, E.; Tanter, C.; Wakx, A.; Dutot, M. A Fast and Reproducible Cell- and 96-Well Plate-Based Method for the Evaluation of P2X7 Receptor Activation Using YO-PRO-1 Fluorescent Dye. *J. Microbiol. Methods* **2017**, *4*, No. e64.
(55) Helliwell, R. M.; ShioukHuey, C. O.; Dhuna, K.; Molero, J. C.; Ye, J.-M.; Xue, C. C.; Stokes, L. Selected Ginsenosides of the Protopanaxdiol Series are Novel Positive Allosteric Modulators of P2X7 Receptors. *Br. J. Pharmacol.* **2015**, *172*, 3326−3340.
(56) Jo, E.-K.; Kim, J. K.; Shin, D.-M.; Sasakawa, C. Molecular Mechanisms Regulating NLRP3 Inflammasome Activation. *Cell. Mol. Immunol.* **2016**, *13*, 148−159.
(57) Barberà-Cremades, M.; Baroja-Mazo, A.; Gomez, A. I.; Machado, F.; Di Virgilio, F.; Pelegrín, P. P2X7 Receptor-Stimulation Causes Fever via PGE2 and IL-1beta Release. *FASEB J.* **2012**, *26*, 2951−2962.
(58) Di, L.; Kerns, E. H.; Fan, K.; McConnell, O. J.; Carter, G. T. High Throughput Artificial Membrane Permeability Assay for Blood-Brain Barrier. *Eur. J. Med. Chem.* **2003**, *38*, 223−232.
(59) Beck, W. T.; Qian, X.-d. Photoaffinity Substrates for P-Glycoprotein. *Biochem. Pharmacol.* **1992**, *43*, 89−93.
(60) Bhattacharya, A.; Wang, Q.; Ao, H.; Shoblock, J. R.; Lord, B.; Aluisio, L.; Fraser, I.; Nepomuceno, D.; Neff, R. A.; Welty, N.; Lovenberg, T. W.; Bonaventure, P.; Wickenden, A. D.; Letavic, M. A. Pharmacological Characterization of a Novel Centrally Permeable P2X7 Receptor Antagonist: JNJ-47965567. *Br. J. Pharmacol.* **2013**, *170*, 624−640.
(61) Letavic, M. A.; Lord, B.; Bischoff, F.; Hawryluk, N. A.; Pieters, S.; Rech, J. C.; Sales, Z.; Velter, A. I.; Ao, H.; Bonaventure, P.; Contreras, V.; Jiang, X.; Morton, K. L.; Scott, B.; Wang, Q.; Wickenden, A. D.; Carruthers, N. I.; Bhattacharya, A. Synthesis and Pharmacological Characterization of Two Novel, Brain Penetrating P2X7 Antagonists. *ACS Med. Chem. Lett.* **2013**, *4*, 419−422.
(62) Jain, S.; Grandits, M.; Ecker, G. F. Interspecies Comparison of Putative Ligand Binding Sites of Human, Rat and Mouse P-Glycoprotein. *Eur. J. Pharm. Sci.* **2018**, *122*, 134−143.
(63) O'Brien, F. E.; O'Connor, R. M.; Clarke, G.; Dinan, T. G.; Griffin, B. T.; Cryan, J. F. P-Glycoprotein Inhibition Increases the Brain Distribution and Antidepressant-Like Activity of Escitalopram in Rodents. *Neuropsychopharmacol* **2013**, *38*, 2209−2219.
(64) Suzuyama, N.; Katoh, M.; Takeuchi, T.; Yoshitomi, S.; Higuchi, T.; Asashi, S.; Yokoi, T. Species Differences of Inhibitory Effects on P-

Glycoprotein-Mediated Drug Transport. *J. Pharm. Sci.* **2007**, *96*, 1609−1618.
(65) Sirimulla, S.; Bailey, J. B.; Vegesna, R.; Narayan, M. Halogen Interactions in Protein-Ligand Complexes: Implications of Halogen Bonding for Rational Drug Design. *J. Chem. Inf. Model.* **2013**, *53*, 2781−2791.
(66) Stock, T. C.; Bloom, B. J.; Wei, N.; Ishaq, S.; Park, W.; Wang, X.; Gupta, P.; Mebus, C. A. Efficacy and Safety of CE-224,535, an Antagonist of P2X7 Receptor, in Treatment of Patients with Rheumatoid Arthritis Inadequately Controlled by Methotrexate. *J. Rheumatol.* **2012**, *39*, 720−727.
(67) Chen, L.; Brosnan, C. F. Exacerbation of Experimental Autoimmune Encephalomyelitis in P2X7R-/- Mice: Evidence for Loss of Apoptotic Activity in Lymphocytes. *J. Immunol.* **2006**, *176*, 3115−3126.
(68) Aldrich, C.; Bertozzi, C.; Georg, G. I.; Kiessling, L.; Lindsley, C.; Liotta, D.; Merz, K. M., Jr.; Schepartz, A.; Wang, S. The Ecstasy and Agony of Assay Interference Compounds. *J. Med. Chem.* **2017**, *60*, 2165−2168.
(69) Kim, H. S.; Ohno, M.; Xu, B.; Kim, H. O.; Choi, Y.; Ji, X. D.; Maddileti, S.; Marquez, V. E.; Harden, T. K.; Jacobson, K. A. 2-Substitution of Adenine Nucleotide Analogues Containing a Bicyclo[3.1.0]hexane Ring System Locked in a Northern Conformation: Enhanced Potency as P2Y1 Receptor Antagonists. *J. Med. Chem.* **2003**, *46*, 4974−4987.
(70) Tobrman, T.; Dvorak, D. Magnesiation of Chloro-iodopurines: an Efficient Approach to New Purine Derivatives. *Org. Lett.* **2006**, *8*, 1291−1294.
(71) Bendels, S.; Grether, U.; Kimbara, A.; Nettekoven, M.; Roever, S.; Rogers-Evans, M.; Schulz-Gasch, T. Purine Derivatives as CB2 Receptor Agonists. WO 2014177490 A1, Nov.6, 2014.
(72) Szarek, W. A.; Pinto, B. M.; Iwakawa, M. Synthesis and Biological Activity of Nucleoside Analogs Involving Modifications in the Carbohydrate Ring. *Can. J. Chem.* **1985**, *63*, 2149−2161.
(73) Grynkiewicz, G.; Poenie, M.; Tsien, R. Y. A New Generation of Ca2+ Indicators with Greatly Improved Fluorescence Properties. *J. Biol. Chem.* **1985**, *260*, 3440−3450.
(74) Gloor, S.; Pongs, O.; Schmalzing, G. A vector for the Synthesis of cRNAs Encoding Myc Epitope-Tagged Proteins in Xenopus Laevis Oocytes. *Gene* **1995**, *160*, 213−217.
(75) Nicke, A.; Kuan, Y.-H.; Masin, M.; Rettinger, J.; Marquez-Klaka, B.; Bender, O.; Górecki, D. C.; Murrell-Lagnado, R. D.; Soto, F. A Functional P2X7 Splice Variant with an Alternative Transmembrane Domain 1 Escapes Gene Inactivation in P2X7 Knock-out Mice. *J. Biol. Chem.* **2009**, *284*, 25813−25822.
(76) Beissner, M.; Dutertre, S.; Schemm, R.; Danker, T.; Sporning, A.; Grubmüller, H.; Nicke, A. Efficient Binding of 4/7 Alpha-Conotoxins to Nicotinic Alpha4beta2 Receptors is Prevented by Arg185 and Pro195 in the Alpha4 Subunit. *Mol. Pharmacol.* **2012**, *82*, 711−718.
(77) O'Boyle, N. M.; Banck, M.; James, C. A.; Morley, C.; Vandermeersch, T.; Hutchison, G. R. Open Babel: An Open Chemical Toolbox. *J. Cheminf.* **2011**, *3*, 33.
(78) Trott, O.; Olson, A. J. Improving the Speed and Accuracy of Docking with a New Scoring Function, Efficient Optimization, and Multithreading. *J. Comput. Chem.* **2010**, *31*, 455−461.
(79) Pettersen, E. F.; Goddard, T. D.; Huang, C. C.; Couch, G. S.; Greenblatt, D. M.; Meng, E. C.; Ferrin, T. E. UCSF Chimera–a Visualization System for Exploratory Research and Analysis. *J. Comput. Chem.* **2004**, *25*, 1605−1612.

https://dx.doi.org/10.1021/acs.jmedchem.0c02145
J. Med. Chem. 2021, 64, 2272−2290